NASA Technical Memorandum 84282

Analysis of Several Glidepath and Speed Control Autopilot Concepts for a Powered-Lift STOL Aircraft

W. S. Hindson

August 1982

National Aeronautics and
Space Administration

NASA Technical Memorandum 84282

Analysis of Several Glidepath and Speed Control Autopilot Concepts for a Powered-Lift STOL Aircraft

W. S. Hindson, Ames Research Center, Moffett Field, California

National Aeronautics and
Space Administration

Ames Research Center
Moffett Field, California 94035

LIST OF SYMBOLS

A	state weighting matrix, n×n
a_x	body axis longitudinal acceleration, m/sec^2
a_z	body axis normal acceleration, m/sec^2
B	control weighting matrix, m×m
C	optimal feedback gain matrix, m×n
C'	modified feedback gain matrix, m×n
d	glidepath error, positive when high, m
$\dot{d}$	glidepath error rate, m/sec
F	system dynamics matrix, n×n
G	control transmission matrix, n×m
H	observation matrix, p×n
I	identity matrix
J	scalar performance index, nondimensional
Q	process noise spectral density matrix, ℓ×ℓ
q	pitch rate, rad/sec
s	Laplace variable, sec^{-1}
T	eigenvector matrix, n×n
u	longitudinal inertial perturbation velocity, m/sec
u_f	complementary-filtered longitudinal velocity error from reference, m/sec
u_w	longitudinal wind disturbance, m/sec
U_0	reference flight velocity, m/sec
$\bar{V}$	complementary-filtered flight velocity, knots
V_{CAS}	flight velocity, knots
w	vertical inertial velocity, m/sec
w_w	vertical wind disturbance, m/sec
$\bar{W}$	vector of process noise disturbances, ℓ×1

X	specific aerodynamic force, x body axis, m/sec^2
$\bar{x}$	vector of system states, n×1
$\bar{x}(0)$	state vector of initial conditions, n×1
$Y_{d\eta_u}$	transfer function from white noise source driving u_w process noise to glidepath error response
$\bar{y}$	observation vector, p×1
Z	specific aerodynamic force, z body axis, m/sec^2
γ_0	reference glidepath angle, -7.5°
γ_I	inertial glidepath angle, deg
δ_e	elevator angle, rad
δ_{ch}	choke position, percent of closure from nominal position
δ_{NH}	engine rpm, percent of maximum speed
δ_ν	nozzle deflection from nominal trim position, rad
$\delta_{\nu_{trim}}$	nominal nozzle angle, rad
δ_{T_c}	throttle position command, deg
Γ	process noise distribution matrix, n×ℓ
$\Lambda(t)$	state transition matrix, u×n
θ	pitch angle, rad
θ_c	commanded pitch angle, rad
ϕ	roll angle, rad
ΔV	filtered speed error from reference value, knots, $\Delta V = -1.94\ u_f$
η_u	white noise source driving u_w process noise
η_w	white noise source driving W_w process noise
σ	root mean square (rms) dispersion statistic
σ'	nominal root mean square parameter used in Ames simulated turbulence model
Φ_{dd}	normalized power spectral density of glidepath error response
$\mathscr{L}\{\ \}$	Laplace transform

$\mathcal{L}^{-1}\{\ \}$ inverse Laplace transform

X state covariance matrix, $n \times n$

ANALYSIS OF SEVERAL GLIDEPATH AND SPEED CONTROL AUTOPILOT CONCEPTS FOR A POWERED-LIFT STOL AIRCRAFT

W. S. Hindson*

Ames Research Center

SUMMARY

A comparison of longitudinal performance and control utilization data is provided for several different automatic-approach autopilot implementations in a powered-lift STOL aircraft. As few as two, to as many as four longitudinal controls are used to manage glidepath and speed with control laws reflecting both backside and frontside control techniques. The data are developed from analysis and simulation, but represent configurations which had actually been demonstrated in flight. Transient response characteristics from initial glidepath offsets are presented, along with performance and control statistics, and spectral content descriptive of system operation in turbulence. In furnishing quantitative data in controlled levels of simulated turbulence, these results provide a useful supplement to various flight investigations (including those employing manual control) that have involved a comparison of control techniques in this type of aircraft.

INTRODUCTION

The choice of a control technique for the management of glidepath and speed in a powered-lift aircraft is influenced by many factors. Beyond the fundamental requirement to produce suitable response characteristics and authorities, are tradeoffs associated with pilot experience and workload capacity, propulsion system and flight control system complexities, and perhaps even passenger ride quality. The choice is generally not a simple one because of the excess number of longitudinal controls that are usually available (e.g., elevator, throttle, fast-acting flaps, direct-lift control devices, vectoring nozzles) and the inability of the pilot to routinely operate more than two of these controls at once. The use of these additional controls (such as those providing low authority direct lift or drag control) is frequently required to improve dynamic response characteristics, or to occasionally achieve greater total authorities of flightpath control. This leads to the requirement for control augmentation systems for manual control, and similar control integration schemes for automatic control.

The use made of the longitudinal controls can be categorized in general as either backside or frontside control concepts. The backside control technique, inherently appropriate for aircraft like powered-lift aircraft whose operating point during approach is typically on the backside of the drag curve, involves the use of throttle for glidepath control, and pitch attitude for speed control. The frontside control technique involves the use of pitch attitude for glidepath control, and some source of longitudinal thrust or drag control to maintain speed. Contributing to the designers' preference for one implementation or the other, or indeed for a combination of the two, are pilot opinion data and operating experience obtained from flight research and pertinent operational aircraft, as well as cost, performance, safety and reliability, passenger ride quality, and mission effectiveness tradeoffs determined from design studies.

---

*Associate Research Officer and Research Pilot, National Research Council of Canada, Ottawa, Ontario. Presently Senior Research Associate, Department of Aeronautics and Astronautics, Stanford University, Stanford, California.

A significant amount of the flight research undertaken with the Augmentor Wing Research Aircraft (AWRA) during its 9 year period of operation at NASA Ames Research Center has contributed to the body of data to assist in these decisions (refs. 1 and 2). In particular, considerable operating experience was obtained in the use of backside and frontside control techniques for the manual instrument approach task (refs. 3-6). Although extensive experience was also accumulated in the use of various automatic approach systems using the backside technique, relatively little effort had been devoted to the study or testing of an alternative frontside automatic control configuration. Consequently, the limited effort reported here was undertaken during the final months of the flight test and fixed-base simulator programs to provide a flight-validated minimal data base for purposes of comparison.

The effort consisted of developing the control structure and gains for a frontside autopilot using a preliminary analytical model in conjunction with a real-time, fixed-base, nonlinear simulation. The resulting control law was validated with a limited flight test before collecting an ensemble of turbulence response data in the fixed-base simulator. The final step in this investigation (unorthodox in sequence as a result of scheduling constraints) was a more detailed analytical study of the frontside and backside automatic control systems that usefully quantified their characteristics for the test aircraft.

In addition to allowing a comparison of various automatic control implementations, it was felt that these data could provide a more quantitative and objective basis to assist in the interpretation of the pilot opinion data for the frontside and backside manual control tests discussed in references 3-6. For example, use of the frontside control technique for low-speed steep approach operations in this type of aircraft has received criticism for involving an excessive amount of pitch activity (refs. 5 and 6). This is primarily a subjective ride qualities consideration, although control authority issues are also involved. Similarly, the backside technique involves levels of throttle modulation for glidepath control that, when added to the installed thrust needed for performance alone, can result in significant design penalties. There are also passenger acceptance considerations associated with unusually high levels and variations in approach thrust, compared with those passengers have come to expect in conventional aircraft. A major objective of this effort was to provide a quantitative basis for evaluating these considerations.

ORGANIZATION OF THE REPORT

Following a brief description of the test aircraft and its longitudinal controls, the report outlines the development and flight validation of control laws for the frontside automatic-glidepath tracking and speed-hold autopilot. The control structures are provided next for two alternative backside-technique autopilots; a simple version employing only two controls, and an advanced version making use of four controls. Transient responses to initial glidepath offsets are calculated from appropriate linear models of each control system. Next, shaping filters are incorporated in the analytical model to permit a calculation of system response characteristics to Dryden turbulence, and these results are compared with probability density data reduced from a large number of fixed-base simulator runs. Representative time histories from the fixed-base simulation are also provided to illustrate the nature of the disturbance functions, performance errors, and the associated control activity. Finally, an optimal control design employing all four longitudinal controls to minimize a weighted sum of specified performance and control variables is included to

demonstrate the utility of linear quadratic optimization methods for dealing with a complex multivariable control system.

The Research Aircraft and Description Of Longitudinal Flight Controls

The Augmentor Wing Research Aircraft is a de Havilland of Canada DHC-5/C8-A Buffalo aircraft, modified with an augmentor flap arrangement as shown in figure 1. The augmentor flap is blown internally by the cold bypass flow from two Rolls Royce Spey 801SF jet engines. This cold flow is cross-ducted to minimize lateral and directional transients in the event of engine failure. The aircraft is described in greater detail in reference 1; it is the longitudinal controls that are of interest in this discussion.

In the powered-lift approach configuration, engine throttle setting determines the magnitude of propulsive-lift generated through the supercirculation action of the augmentor flap. The residual hot thrust from each engine is exhausted through the rotatable nozzles seen in figure 2. When vectored to a downward position during steep approach, these nozzles conveniently provide for ample reduction in longitudinal forces while maintaining the moderate power settings necessary to provide propulsive lift. When modulated about their deployed position (typically 70° relative to aircraft datum), these nozzles can also furnish significant control of longitudinal force without causing any major effect on lift, and consequently are of considerable utility for speed control, or for long term glidepath control. As seen in figure 3, the throttles and the nozzles each provide the same order of control authority measured in terms of available flightpath angle when the other control remains fixed. Indeed, two of the control law implementations analyzed here involved these cases, which reflect essentially the backside and frontside control techniques. Since this study addressed only small perturbations about the nominal approach condition, further discussion of issues associated with control authorities is not included, but may be found in references 5 and 6.

Located within the inboard augmentor flap segments are electrohydraulically actuated surfaces which can serve to choke the flow through the augmentor flap, thereby providing a significant amount of rapidly responding direct-lift control. When used for this purpose, the chokes are typically operated over a range of ±30% of full closure from a bias position of 30%, where they generally require an additional 1.5% of engine rpm in order to maintain the trim glidepath angle. These chokes are not directly available to the pilot for manual actuation, but can be incorporated into various automatic control or stability augmentation schemes.

While the setting of the augmentor flap potentially provided a fifth longitudinal control device for integration, its use was impractical on account of its slow rate of actuation. The augmentor flap was considered a configuration control only, and was routinely positioned at 65° for the -7.5° glideslope and 70 knot approach conditions considered here.

A flexible digital avionics system was installed in the aircraft including the features shown in figure 4. A 32K/18-bit-word minicomputer performed navigation, guidance and control requirements through interfaces with electronic servos, cockpit displays, and the pilot's mode selection panel. This system, also included in the fixed-base simulator to assist in development of the flight software, was used to incorporate the various glidepath tracking automatic control laws that are the subject of this report.

Frontside Autopilot Development and Flight-Test Documentation

The frontside control system is characterized by the assignment of pitch attitude to glidepath control, nozzle modulation to speed control, and fixed throttle setting. A wide-bandwidth, high authority speed-control system that had been developed for an earlier manual-control investigation (ref. 5) was used to provide the necessary speed stabilization. Simple proportional, derivative, and integral gains were incorporated for glidepath tracking as shown in figure 5.

The speed-hold system shown in figure 6 included a heave-damping augmentation feature, and incorporated a crossfeed from the nozzle position to the augmentor chokes, scheduled so as to approximately offset the small loss in lift that occurs whenever the nozzles are retracted. The system is described in greater detail in references 5 and 6.

A simplified linear stability analysis, which ignored both pitching-moment dynamics and servomechanism dynamics, was carried out to determine the closed loop glidepath control gains K_5, K_6, and K_7. A limited range of these gains was then briefly evaluated in the real-time flight simulation facility in the presence of turbulence. Unlike the simplified analytical model, the simulation included nonlinear aerodynamics, a model of the pitch control system, and electromechanical servo models that incorporated the rate and authority limits of the flight hardware (refs. 7 and 8). MLS beam noise was not simulated. This was justified since the beam-deviation and beam-rate feedback signals, d and $\dot{d}$, were obtained from a third-order complementary filter that removed most of this noise (ref. 9). Finally, two short test flights were undertaken to validate the best control-law configuration. It was this flight-validated configuration that was then used to produce the more extensive analytical and simulation data contained in this report.

Figure 7 presents two approach time histories from these system-validation flight tests that used the path-tracking gains shown in table 1. The atmospheric turbulence encountered during these flights was of light intensity.

Backside Autopilot Configurations

Unlike the frontside autopilot which was quickly incorporated and only briefly flight tested, the backside control configurations had received extensive simulator development and flight evaluation (refs. 8 and 10). Two variations of this backside autopilot were chosen to provide the comparative data needed for this study.

The simplest implementation of the backside automatic glidepath tracking system involved the use of engine power for flightpath control, and pitch attitude for speed control. For this "two control" configuration, the nozzles were fixed at a trim setting near 70°, except when significant changes in mean along-track winds required an adjustment in trim drag in order to keep engine power settings within an acceptable range.

A more advanced "four control" configuration used the nozzles for speed control, and integrated the chokes into the height-control loop to provide improved glidepath response at frequencies higher than the engine-control loop alone could provide. Pitch attitude was driven by the integral of speed error, effectively performing the longitudinal trim function.

The closed-loop control structure for both versions is shown in figure 8. The "two control" configuration is obtained by setting gains K_4 and K_5 to zero and altering the remaining gains and time constants as indicated in table 1.

Model Equations and Time Histories

General- The usual method for assessing the performance of regulator-type control systems, such as autopilots, is to describe their ability to carry out the regulation task in the presence of typical or severe levels of externally applied disturbances, such as turbulence or guidance-system noise. This requires a model of the disturbance functions, and the results of such an analysis are most often stated in terms of statistical (rms) measures of system performance and control utilization, and additionally, power-spectral responses to the applied disturbances. This analytical approach is used for the case of atmospheric turbulence in a subsequent section. However, it is useful first to provide an equally relevant description of system performance and stability, namely, the time response to an initial offset that could occur during initial engagement. The condition employed here is a 5 m (15 ft) initial offset below the glidepath, from which characteristic response times, control activity, and inherent stability can be assessed with meaningful physical significance.

The important features of each configuration were represented by linear models as summarized below, from which time-history response characteristics were calculated. For completeness, the characteristic roots for each configuration and the residues for the various responses to the initial condition in d are recorded in table 2.

Frontside configuration- The analytical model described here was more extensive than the simplified model used in the early stages of the development of outer loop gains for the flight validation. Nevertheless, dynamics and nonlinearities associated with the elevator, nozzle, and choke servos have been ignored in this analysis, an assumption which would only seriously affect the nozzle servo loop, which in the actual system exhibited a maximum rate capability of 20°/sec. (The characteristics of the parallel electromechanical elevator and nozzle servos, and the electrohydraulic choke servos, are summarized in reference 8. They were essentially those which were also incorporated in the fixed-base simulator. Their bandwidths are considered to be sufficiently above the control frequencies of interest to justify omission.)

However, the frontside analysis detailed below does contain a model of the inner-loop pitch-axis dynamics, deemed necessary in view of the significant pitch-control activity to be expected in this configuration. The models for the speed-hold and heave-augmentation system, and the glidepath tracking laws, are those shown in figures 5 and 6. The resulting model equations in Laplace notation are:

Aircraft:

$$su = X_u u + X_w w + X_{\delta_\nu}\delta_\nu + X_q q - g\cos\gamma_0\theta$$

$$sw = Z_u u + Z_w w + Z_{\delta_\nu}\delta_\nu + Z_{\delta_{ch}}\delta_{ch} + (U_0 + Z_q)q + Z_{\delta_e}\delta_e - g\sin\gamma_0\theta$$

$$sq = M_u u + M_w w + M_{\dot{w}} sw + M_{\delta_\nu}\delta_\nu + M_q q + M_{\delta_e}\delta_e$$

Attitude Stabilization and Command System:

$$\delta_e = K_q q + K_\theta(\theta - \theta_c)$$

Speed-Hold System:

$$\left(K_1 + \frac{K_2}{s}\right) u + \left(\frac{K_3 \tau_3 s}{\tau_3 s + 1}\right) \theta + \delta_\nu = 0$$

Heave Augmentation:

$$\left(\frac{K_4 \tau_4 s}{\tau_4 s + 1}\right) \theta + \delta_{ch} = 0$$

Kinematic Relationships:

$$s\theta = q$$

$$sd = U_0 \theta - w$$

Glidepath Control:

$$K_5 d + K_6 sd + K_7 \frac{d}{s} = \theta_c$$

In the aircraft, the path-deviation signals, d and sd, were derived from a third-order complementary-filter implementation, documented in reference 8, which furnished smoothed data of high bandwidth from measurements of MLS elevation and azimuth angles, precision DME range, and normal acceleration in runway coordinates. Consequently, perfect position feedback data is assumed. Similarly, the actual speed-hold system in the aircraft employed a second-order complementary filter, as shown in figure 6, to suppress the effects of atmospheric turbulence on the velocity feedback signal. This filter was not included for any of the configurations at this stage of the analysis; it was included for the turbulence-response analysis considered subsequently.

The reference flight condition and the corresponding stability derivatives were based on the data of reference 8, and are listed in table 1. For the frontside autopilot analysis, Z_{δ_ν} was simply set to zero, since changes in lift associated with nozzle rotation were compensated by an appropriate choke crossfeed as shown in figure 5. The speed-hold system gains and time constants K_1, K_2, K_3, K_4 and τ_3, τ_4 are shown in figure 6, and the path-tracking gains are indicated in table 1. The ninth-order linear system represented by these equations is provided in state variable format in the appendix (table A1).

The performance of this frontside-automatic control system is characterized by the time response of the system, measured by d, u, θ, δ_{ch}, and δ_ν, to an initial offset of 5 m (15 ft) below the glidepath. The responses are presented in figure 9, and show response times, stability characteristics and control activity that will be compared with the backside configurations, to be considered next.

Backside configurations- The aircraft model employed for the linear analysis of the backside glidepath tracking configurations consisted of the X and Z force

equations, with appropriate engine control terms added. The pitching-moment equation was justifiably eliminated (with the result that $\theta = \theta_c$) on account of the significantly smaller amplitude and lower frequency control activity inherent with this control technique. Such a simplification is often made for STOL aircraft equipped with a high-gain pitch-attitude stabilization loop, and is analytically justified in reference 3. The corresponding pitch rate and elevator derivatives in the X and Z force equations were also deleted.

During the extensive backside-autopilot flight-test investigations reported, in part, in reference 10, it was found that the bandwidth of control available from the throttle servo and engine system had a significant effect on the quality of glidepath tracking which could be achieved. Of importance were the maximum rate capability of the servo (6.28°/sec), a hysteresis band approximately 1% wide in the linkage between the throttle servo and the engine fuel control unit, and nonlinear engine dynamics. These nonlinearities were accounted for in the simulation studies reported in reference 8 but are ignored for this analysis which employed instead the second-order servo and engine model shown in figure 10.[1] Because of these response lags associated with throttle control, the glidepath control laws for the more advanced "four control" configuration shown in figure 8 reflect the design objective to complement the engine response with high-passed direct-lift control provided by the augmentor chokes. To meet this objective, the choke gain K_5 was chosen, to approximate $Z_{\delta_{NH}}/K_1 Z_{\delta_{ch}}$. No other servo systems were modeled for the analysis reported here.

The model equations descriptive of the backside "two control" configuration, characterized by throttle and pitch-control utilization alone with nozzles and chokes fixed or unused, are:

Aircraft:

$$su = X_u u + X_w w + X_{\delta_{NH}} \delta_{NH} - g \cos \gamma_0 \theta$$

$$sw = Z_u u + Z_w w + Z_{\delta_{NH}} \delta_{NH} + U_0 s\theta - g \sin \gamma_0 \theta$$

Throttle Servo and Engine Dynamics:

$$\frac{\delta_{NH}}{\delta_{T_c}} = \frac{2.88}{s^2 + 2(0.7)s + 2^2}$$

Speed Control:

$$\theta = K_3 u + K_2 \frac{u}{s}$$

---

[1]Some variations in the servo-engine system damping, and in the outer-loop glidepath control law gains were made for the flight-tested and simulated backside configurations. For example, the "four-control" configuration was more accurately described by a servo-engine system damping ratio of 0.9 instead of 0.7, and proportional integral, and damping glidepath gains which were each 89% of those quoted in table 1. These changes had little influence on the analytical results reported here.

Glidepath Control:

$$\delta_{T_c} = \left(\frac{K_6 s^2}{\tau_6 s + 1}\right) d + K_7 sd + K_8 d + K_9 \frac{d}{s}$$

Kinematics:

$$sd = U_0\theta - w$$

The "four control" configuration involves the addition of nozzle and choke stability derivatives to the X and Z force equations and changes in the speed and glidepath control laws as shown in figure 8. The eighth-order state variable systems used to obtain the time-history responses for both backside configurations are contained in the appendix (tables A2, A3).

Aircraft:

$$su = X_u u + X_w w + X_{\delta_\nu} \delta_\nu + X_{\delta_{NH}} \delta_{NH} - g \cos \gamma_0 \theta$$

$$sw = Z_u u + Z_w w + Z_{\delta_\nu} \delta_\nu + Z_{\delta_{NH}} \delta_{NH} + Z_{\delta_{ch}} \delta_{ch} + U_0 s\theta - g \sin \gamma_0 \theta$$

Throttle Servo and Engine Dynamics:

$$\frac{\delta_{NH}}{\delta_{T_c}} = \frac{2.88}{s^2 + 2(0.7)s + 2^2}$$

Speed Control:

$$\theta = K_2 \frac{u}{s}$$

$$\delta_\nu = K_4 u$$

Glidepath Control:

$$\delta_{T_c} = K_7 sd + K_8 d + K_9 \frac{d}{s}$$

$$\delta_{ch} = \left(\frac{K_5 \tau_5 s}{\tau_5 s + 1}\right) (\delta_{T_c} - K_1 \delta_{NH})$$

The time-history responses for an initial 5 m (15 ft) offset below the glidepath are shown for the two backside configurations in figure 9. Deferring comparison with the frontside-system characteristics until later, it is seen that the glidepath error transients, which are plotted in figure 9, illustrate similar stability characteristics as demonstrated by convergence to the glidepath, but show a significantly faster initial-response time for the "four control" system. This is due to the action of the chokes in providing an immediate lift increment without having to suffer delays involved in the throttle servo and engine dynamics. (The initial choke deflection determined by the analysis exceeds the ±30% control authority available making the glidepath response calculated for the "four control" system unrealistically good.) The amount of throttle activity for each system is about the same, while the speed- and pitch-angle excursions are so small as to be negligible.

Comparison of frontside and backside time response characteristics- When all three systems are compared on the basis of the glidepath convergence shown in figure 9, the "two control" backside configuration is seen to have the slowest response as measured by the time to half amplitude. The other two configurations, which make use of additional controls, show very similar characteristics. The initial delay exhibited by the frontside system is primarily a result of the particular mechanization of the chokes for providing heave augmentation, which involved actual, rather than commanded pitch attitude. Hence, their effectiveness was slowed considerably in comparison to the "four control" backside configuration, where a term directly proportional to the throttle-command signal produced immediate choke response to glidepath error signals. It is worth reminding the reader that the response of the frontside system is obtained without any use of throttle, while the backside configurations make very little use of pitch attitude. For all three configurations, a glidepath overshoot of approximately 10% occurs before the path error is nulled.

It is apparent that the three control techniques described in this study are not entirely consistent in their implementation. On the one hand, the frontside system and the backside "two control" system are similar in that they can be automatic control implementations of configurations that can be flown manually, provided the frontside heave-augmentation system remained automatic. That is, only two controls (pitch attitude and throttle) would require manipulation, and the chokes, when used with the frontside technique, remain dependent on pilot-effected pitch control for their actuation. Flight investigations of these two manual-control techniques have been carried out (refs. 4 and 6), and this study, although involving an automatic pilot, is useful to provide additional data on their inherent characteristics. Alternatively, when these two configurations are viewed only as automatic control systems, the backside "two control" configuration appears to be disadvantageous on the basis of system response time, although it does permit a relatively simple implementation. However, the determination of a STOL control technique appropriate to automatic and manual operation goes well beyond the system-performance considerations emphasized in this work, to include pilot-related considerations, ride-quality factors, control authority including installed thrust requirements, control system complexity, and system reliability.

On the other hand, the backside "four control" configuration is exclusively an automatic-control implementation since the chokes were controlled directly by the glidepath error, not in a way the pilot could manage. Although this configuration and the frontside configuration are similar in the sense that the chokes are used in both systems, a fair comparison could only be drawn if the chokes were driven directly by glidepath error in each case. On the basis of the initial-path responses shown in figure 9, however, this particular inconsistency does not appear to be of serious consequence.

System Performance in Turbulence

General- The three glidepath and speed-control autopilots are compared in this section on the basis of their response to turbulence. Data obtained from an ensemble of runs using the full six-degree-of-freedom nonlinear simulation model are first presented in the form of probability density or amplitude-distribution histograms, from which rms performance and control-utilization measures are obtained. These data are then compared and supplemented with analytical results obtained from the same linear models described previously, but expanded to include representations of the disturbance spectra and the second-order complementary airspeed filter used in the aircraft for turbulence rejection.

Simulation results- The atmospheric turbulence model used for these tests was the Dryden spectral form, conforming for the most part to specifications contained in reference 11. While it might have been preferable to modify the turbulence model to suppress its altitude-dependent variations encountered during the descending approaches (that generally ran between 450 m and 60 m), this was not done. Hence, stationarity does not quite prevail for the tests that were conducted. Figure 11 shows the "altitude-averaged" gust amplitude-distribution histograms and associated rms levels that were produced by the turbulence model for an ensemble of 43 simulated approaches. The programmed altitude variation in the gust-component dispersions is also noted in the figure.

The physical nature of the aircraft responses and control activities to the simulated turbulence for each of the three simulated autopilot systems is illustrated by the typical time histories presented in figure 12. While amplitude-distribution histograms (presented next) provide a better summary of characteristic dispersions in the performance and control parameters that also are evident in the time histories, it is the frequency content (particularly in control activity) that should be noted qualitatively. Although this too will be quantified later, the reader should note the markedly different character of the nozzle, throttle, and pitch controls for the separate concepts. For the frontside configuration, figure 12(a), the somewhat oscillatory nature of the nozzle control activity that appears at a frequency near 1 rps is partially a result of the 20°/sec maximum servo rate-limit that was programmed in the simulation. Similarly, a throttle rate-limit of 6.28°/sec was frequently encountered during simulation and flight test runs, and is probably somewhat responsible for the 1 rps frequency content also evident in the two-control backside configuration. The choke activity also occurs at fairly high frequency for the frontside and four-control backside configurations, but is in no way objectionable since the action of the chokes is scarcely perceptible to the pilot. The bias position of the chokes for the frontside configuration shown in figure 12(b) was erroneously set at 40% during this run. Nevertheless, ample travel within the 0% to 60% available authority remained. However, the moderate turbulence level used for these tests was sufficient to cause near-saturation of the chokes even when properly positioned at their 30% setting for the four-control backside configuration, figure 12(c). This suggests that the design criteria, discussed previously, that was used to determine the choke gain, should be altered to take into account the limited control authority available.

The amplitude distribution of the pertinent longitudinal performance and control parameters for a conglomerate of many runs in each of the three configurations is presented in figure 13. The main result is that nearly identical performance, measured in terms of beam deviation, d, and speed error, ΔV, is achieved by both the frontside configuration and the four-control backside configuration. The backside configuration that used only two controls was markedly inferior, but still provided adequate performance. With these performance comparisons in mind, the relative amounts of control involved in achieving these levels can be weighed.

One method of interpreting the amplitude-distribution data shown in figure 13 is in terms of control power requirements. For example, three-sigma nozzle control power requirements for the frontside system tested in the level of turbulence used in this simulation are approximately $Z_{\delta_\nu}\delta_{\nu_{3\sigma}} = 0.11$ g, approximately twice that encountered for the four-control system. Similarly, it is seen from the rms activity levels of the primary glidepath control (pitch attitude for the frontside system, figure 13(a), and engine rpm for the two backside configurations, figures 13(b) and (c)), that there is a close equivalent of a degree of pitch attitude to a percent of engine rpm. This, of course, reflects the system gains, that in turn reflect the basic control

effectiveness seen in the $V - \gamma$ plots of figure 3. However, the correspondence also loosely conforms to what the pilot might be expected to accept (or use) for an automatic (or manual) control system from a ride-qualities or pilot-acceptance point of view. Stated differently, it could be inferred that a 5° excursion in pitch attitude would be undesirable as a 5% change in rpm, a conclusion which was roughly corroborated during, or perhaps evolved from, extensive experience in the test aircraft.

Analytical results- The previously described linear analytical models for the three autopilot configurations were expanded to include representations of the atmospheric turbulence, and a turbulence suppression airspeed filter that had been incorporated in the flight and simulation software. Using the method developed in reference 12, the longitudinal and vertical gust components were modeled with first-order shaping filters driven by white noise. The parameters for the Dryden turbulence model used in defining these shaping filters were those which approximately matched the altitude-averaged rms gust intensities derived from results determined in the simulation tests. The resulting expressions (representing the Dryden model at an altitude of 290 m with longitudinal and vertical rms gust intensities of 1.09 m/sec and 0.89 m/sec respectively) are

$$\dot{u}_w = -0.195(u_w - \eta_u)$$

$$\dot{w}_w = -0.443(w_w - \eta_w)$$

where η_u, η_w represent white noise with zero mean values and spectral densities 12.2 and 3.58 m^2/sec respectively.

Figure 6 shows the second-order complementary airspeed filter which was incorporated to suppress some of the turbulence in the feedback signal used in the autopilot speed-control loops. (A detail to note is that only the proportional speed error terms used this filtered quantity; the integral terms used raw airspeed.) The filter equation is

$$\frac{s^2 u}{(s + 0.25)^2} + \frac{0.5(s + 0.125)(u - u_w)}{(s + 0.25)^2} = u_f$$

Alternatively,

$$\dot{u}_f = x_3$$

$$\dot{x}_3 = \frac{d\dot{u}}{dt} + 0.5(\dot{u} - \dot{u}_w) + 0.0625(u - u_w) - 0.0625\, u_f - 0.5\, x_3$$

which can readily be put into state-variable form upon appropriate (but lengthy) substitution for the terms $d\dot{u}/dt$ and $\dot{u} - \dot{u}_w$ obtained from the previous gust models and the basic lower-order autopilot models detailed in the appendix. The addition of the two gust states, and the two states associated with the second-order airspeed filter, results in twelfth and thirteenth order linear stochastic models for the backside and frontside configurations respectively. The models are solved (see appendix) to yield performance and control covariance (mean square) estimates and power-spectral density functions.

A comparison of the rms statistics from this analysis with those obtained in the simulation investigation is presented in table 3. Reasonable agreement prevails; this is not surprising in the light of the low-disturbance levels used and the near-equivalence of the experimental (simulation) and analytical methods for small amplitude motions. The largest discrepancies occur in the complementary-filtered speed error statistics, for which the nonstationary nature of the disturbance used in the simulation may be significant. In addition, there were some minor differences in the simulation control-law gains for the backside configurations compared to the ones used for the analysis. These were mostly required to reduce the bandwidth of the inner control loops (pitch and throttle) so oscillatory problems associated with the various compute cycles of the digital-simulation program would not appear. However, the analytical gains were essentially those used in flight for all configurations.

The reasonable comparisons of rms control activity provide some confidence in the analytical power-spectral densities of the performance and control parameters which are considered next. These were calculated using the method described in the appendix. They reflect the dominant control input and aircraft response frequencies for selected variables in each configuration as shown in figure 14. The input turbulence spectra are shown for completeness in figure 15. As expected, the higher frequency control activities near one rps that were discussed earlier in connection with the simulation time histories do not appear in the spectral analysis, since their source is not part of the linear models. For all configurations, the dominant glidepath response and associated primary-controller frequencies are in the range 0.1 to 0.2 rps. The two-control backside configuration has both the longest characteristic periods and the largest performance and control dispersions. (Note that the normalized power spectra presented in figure 14 require interpretation in conjunction with the rms statistics shown in table 3.)[2]

These data indicate that the quantitative differences among the three control configurations considered here are not major. That is, the frequency content and the control effectiveness (the latter characterized by rms dispersions in pitch, nozzle, and throttle) are all similar. Yet the differences among the control configurations are significant from a subjective ride-qualities or pilot-acceptance point of view. As discussed in reference 5, there are fundamental physical differences between pitch-control activity and throttle activity. Pitching activity is strongly apparent to the pilot or passenger through visual and angular and linear vestibular cues, while throttle or nozzle control activity is probably less apparent since mainly just aural and linear vestibular cues are involved. It might be expected that pitch control activity, at the levels characteristic of low-speed frontside-control configurations, could be more objectionable than throttle control of equivalent effectiveness. This was generally found to be the case by the research pilots who have evaluated these concepts during the flight tests reported here and in references 4-6. In some cases, the level of pilot acceptance was influenced by previous experience in low-speed aircraft or helicopters. The following section considers a control

---

[2]The absence of dc power in the u_w wind component of the longitudinal controls in all of the configurations is a consequence of the kinematic relationship $\dot{d} = -w + U_0\theta$ used in the linear model. In the absence of a vertical wind, this expression forces control to an airmass referenced glideslope for which, in a steady horizontal wind, the trim control positions do not change. Conversely, a steady vertical wind alone will be countered by small control biases in an attempt to maintain the same inertial glidepath. This inconsistency cannot be resolved within the framework of a linear analysis, where the assumption $U_0 + u \doteq U_0$ is made, and the objective of controlling to an inertially fixed glidepath is implicit but not exact.

configuration making "optimum" use of all four longitudinal controls (minimizing the amount of pitch-control activity characteristic of the frontside configuration while increasing the minimal utilization of it as incorporated in the four-control backside configuration).

An Alternative Control Law

The three automatic control laws that have been described in this report were developed, for the most part, using engineering interpretation of piloted simulation and flight-test results, rather than using comprehensive analytical techniques. One reason for the heavy emphasis on simulation was the unusual redundancy of longitudinal controls in the research aircraft, where four different devices were potentially available to regulate glidepath and speed errors. The piloted simulation naturally induced a basic simplification of candidate control law structures that were in accordance with the backside and the frontside control techniques. Eventually, the more desirable features of both control techniques were combined, resulting in the "four-control" backside configuration described earlier. This design process was lengthy in that several control law structures had to be defined and evaluated before the merits of control integration could be assessed. Indeed, the same procedure would have been necessary had classical analytical techniques played a major role in the synthesis of control laws.

Alternatively, modern optimal control synthesis methods (ref. 13) permit a rapid, single-step solution to complex multi-input, multi-output, closed-loop control problems. Specific control-loop structures do not need to be defined or assumed. Nevertheless, considerable judgment is still required in the specification of weighting parameters used in the analysis, and several design iterations are usually necessary to meet design goals.

For the flight control problem considered here there is potentially a more effective use of all four controls, so as to make available the maximum amount of control power for dealing with extreme disturbances without encountering control saturation. Of similar benefit is the capability to systematically adjust the trade-offs in control activity. This provides a solution to the problem areas described earlier for the frontside- and backside-control techniques, where each suffered from the inefficiencies and adverse ride qualities associated with the sometimes excessive use of one control, while another equally powerful control was underutilized. For example, variations in engine-noise levels and installed-thrust requirements perhaps could be reduced in exchange for some acceptable level of pitch-control activity during approach.

A control law was synthesized using these techniques as summarized in this section and in the appendix. However, the resulting design was not tested using the nonlinear simulation, or in flight. Nevertheless, comparison with the linear analytical models developed earlier to document the frontside- and backside-control systems, serves to provide a means for assessing the validity of this alternative control law.

Details concerning the aircraft and control system model used for this analysis are contained in the appendix. Pertinent system limitations had to be taken into account since the objective of the analysis procedure was to determine a practical use of all four longitudinal controls that would provide good performance. Briefly, the throttle servo and engine dynamics were modeled as previously described, and a 2 sec washout on the chokes was incorporated in recognition of their limited authority,

and to ensure their use for higher frequency control requirements. The basic pitch axis dynamics of the aircraft were also included, thus incorporating (perhaps unnecessarily) the design of what was formerly the inner-loop pitch-command system into the overall control-law synthesis procedure. Finally, integral states were provided for speed and glidepath error to ensure zero offsets in those parameters for any implementation involving, inevitably, omissions or errors in modeling.

For a linear system described by

$$\dot{\bar{x}} = F\bar{x} + G\bar{u}$$

the synthesis procedure first determines a full-state feedback control law of the form

$$\bar{u} = -C\bar{x}$$

which is considered to be optimal in the sense that it minimizes the scalar quadratic performance index J:

$$J = \lim_{t\to\infty} \int_0^{\infty} [\bar{x}^T A\bar{x} + \bar{u}^T B\bar{u}]dt$$

A and B are weighting matrices (assumed diagonal) that influence the relative amount of activity permitted in each of the system states and in the controls. The choice of these elements is the principal means whereby engineering judgment is introduced to the synthesis, and represents an indirect method for specifying the system-response characteristics. For this case, the following weights were chosen in the manner recommended in reference 13, using significant a priori knowledge of the system.

State, X_i	Chosen nominal value, X_0	Weight, $1/X_0^2$
u	1.5 m/sec	0.444
$\int u$	.1 m	100
$-\dot{d}$	unconstrained	0.0
d	3 m	.111
$\int d$	0.095 m/sec	111.0
q	unconstrained	0.0
θ	1.48°	1,500
$\dot{\delta}_{NH}$	unconstrained	0.0
δ_{NH}	0.71%	2.0
δ_{ch}	25%	.0016

Control, u_i	Nominal value, u_0	Weight, $200/u_0^2$
δ_e	4°	86,200
δ_{T_c}	1.25%	256
$\dot{\delta}_{ch}$	28%/sec	0.5
δ_ν	14.4°	6,400

The common factor of 200 used for the control weights was chosen to adjust the characteristic response time of the system (for an initial glidepath error) to values similar to the previous configurations shown in figure 9.

The eigenvalues of the closed-loop system,

$$\dot{\bar{x}} = [F - GC]\bar{x}$$

and the feedback gains, C, determined at this stage of the analysis are shown in table 4.

A significant disadvantage of this control synthesis technique is that an unusual number of feedback gains must be implemented. Nowadays, this is usually not a problem in terms of adequate on-board computing power; instead, reliable measurements of all the necessary states may not be available. Frequently, a Kalman filter must be implemented to smooth noisy measurements of the system states or, equally important, to reconstruct from a system model those states not measured. Fortunately, most aircraft system states are routinely available, with the result that implementation is possible without the need for a Kalman filter.

In this example, good quality measurements of all states except the time derivative of engine rpm were available on the research aircraft. Consequently, a fairly good design can be obtained by starting with the full-state feedback gain matrix, setting the $\dot{\delta}_{NH}$ gains to zero, and making minor adjustments as necessary in some of the other gains. A more rigourous method would involve use of dynamic programming techniques to force the gains on the unavailable states to zero from their initial values determined from a full-state optimal synthesis (refs. 14 and 15). Following several trials necessary to restore some lost damping, the eigenvalues and feedback gains for the modified feedback gain matrix were finalized as shown in table 4. The time response of this system to an initial 5 m (15 ft) offset below the glidepath is shown in figure 16. The response times are similar to those for the frontside and backside configurations, proven by flight-test to be characteristic of an acceptable system. The overshoot in glidepath error is somewhat greater (35% vs the 10% representative of the other configurations) and is probably a result of the initial engine rpm transient which peaks at 2.6% in less than 1 sec, rather than the slower response (3.0% in 2 sec) shown in figure 9(b) for example, for the two control backside configurations. In retrospect, increasing weighting on $\dot{\delta}_{NH}$ or on δ_{T_c} in the performance index would be appropriate to constrain throttle activity to lower levels. To pursue this problem further, the throttle servo-rate limit of 6.28°/sec that existed in the aircraft could have been accounted for in the analysis by incorporating δ_{T_c} as an additional state, and defining $\dot{\delta}_{T_c}$ as the control input, using appropriate weightings throughout. Alternatively, increased weighting on $\dot{d}$ would also have the effect of slowing system response.

To evaluate the performance of this system when subjected to the same turbulence inputs used for the frontside and backside configurations, the model was expanded in an identical way to include the turbulence-shaping filters and the second-order airspeed filter. The fourteenth order system is detailed in the appendix in the form

$$\dot{\bar{x}} = [F - GC']\bar{x} + \Gamma\bar{w}$$

where C' is the reduced order feedback gain matrix shown in table 4. The resulting state rms statistics are shown in table 3, and indicate the extent to which <u>both</u> throttle and pitch control are used in realizing levels of system performance similar to that achieved by the frontside and backside configurations. Selected power spectral densities of states and controls are shown in figure 17. The results are similar to the classical configurations, with the exception that glidepath errors and engine

rpm activity occur at higher frequencies because of the excessively active throttle and lower damping mentioned earlier.

Although further iterations of this design along the lines suggested earlier are warranted, the potential of this procedure particularly for powered-lift aircraft having redundant longitudinal controls is apparent. System sensitivity to nonlinearities and modeling errors, and sensor or servo system failures are among many additional factors that would have to be considered in any serious design effort.

CONCLUDING REMARKS

This report has provided an analysis of four different glidepath and speed-control autopilot configurations for a powered-lift STOL aircraft using as many as four different longitudinal controls simultaneously. The configurations ranged from a simple autopilot with only two controls using a backside-control technique, to a fully integrated but easily synthesized configuration using all four controls in a mechanization involving nearly full-state feedback. Three of the four configurations had been validated in-flight, while the fourth configuration is considered reasonable on the basis of similarity.

The objective of the analyses, in addition to providing documentation of flight-tested configurations, was to quantify and compare the levels of control activity involved in the various configurations in the presence of specified disturbance inputs. (The performance of all four systems was shown to be roughly comparable.) The control requirements so determined comprise only some of many factors to be taken into account when defining a control technique appropriate to a powered-lift aircraft. Despite the demonstration that similar levels and frequencies of pitch and throttle control utilization were involved in their respective configurations, it was observed that ride-qualities or pilot-acceptance considerations may strongly influence the desirability of some of these configurations. In particular, the subjective evidence from accumulated flight experience with these configurations highlighted the preference for constraining pitch-control activity to levels below that which would be associated with the frontside-control configuration studied. Since two of the control configurations (the frontside and the "two control" backside systems) required the independent active manipulation of, at most, only two controls, the data also provide useful supplementary information on control activity and ride quality levels perhaps pertinent to the case of piloted operation.

The analysis of these automatic control configurations is not exhaustive but merely provides insight into some of their features. The effects of nonlinearities and other modeling errors, the response to deterministic or "worst-case" windshears and to numerous types of systems failures, are among many factors that require detailed consideration.

APPENDIX

State Variable Analysis of the Automatic Control Configurations

The aircraft and control system models summarized in the main body of this report were converted from their Laplace representation to the standard state variable format

$$\dot{\bar{x}} = F\bar{x} + G\bar{u} + \Gamma\bar{w} \; ; \qquad \bar{y} = H\bar{x} \tag{A1}$$

where

$\bar{x}$ is the vector of system states and F the system matrix

$\bar{u}$ is the control vector and G the control transmission matrix

$\bar{w}$ is the disturbance vector and Γ its transmission matrix

$\bar{y}$ is the observation vector and H the matrix describing its construction from the system states

For a closed loop control system from which control laws are formulated as linear combinations of system states, $\bar{u} = -C\bar{x}$, an alternative representation is

$$\dot{\bar{x}} = [F - GC]\bar{x} + \Gamma\bar{w} \tag{A2}$$

Tables A1, A2, and A3 detail the system matrices and system states that were used for the analysis of the frontside- and backside-autopilot configurations. In the case of the frontside configuration the system matrix represents the aircraft including the speed-hold and heave-augmentation systems, but without the glidepath loop closed. Hence in this case, the form (A1) was used initially with $\bar{u} = -C\bar{x}$ corresponding to $\theta_c = K_5 d + K_6 \dot{d} + K_7 \int d$. Subsequently, and for both the backside configurations, the system matrix included all the feedback-control laws in the form represented by (A2).

The time response characteristics to initial offsets were determined from a modal analysis of the closed-loop homogeneous systems. Essentially,

$$\bar{x}(t) = T\Lambda(t)T^{-1}\bar{x}(0)$$

where T is the eigenvector matrix, T^{-1} its inverse, and $\Lambda(t)$ the block-diagonal modal-transition matrix involving the system eigenvalues, determined from

$$\Lambda(t) = \mathcal{L}^{-1}\{(sI - T^{-1}FT)\}$$

The covariance estimates and spectral-density functions were obtained from the basic system models, expanded to include u_w and w_w gust states, and a second-order complementary airspeed filter. These representations were described in the main text. For the statistically stationary process assumed here, the state covariance matrix χ is the solution to the Lyapunov equation:

$$F\chi + \chi F^T + \Gamma Q \Gamma^T = 0$$

where Q is the matrix of the power spectral densities for the white noise sources driving the turbulence shaping filters. The mean square dispersions of the system performance and control parameters are the diagonal terms of the matrix $H\chi H^T$.

Normalized power spectral density functions were determined from these higher order models using the method outlined in reference 15. For example,

$$\hat{\Phi}_{dd} = \frac{1}{\pi\sigma_d^2}\left\{Y_{d\eta_u} Y^*_{d\eta_u} \Phi_{\eta_u\eta_u} + Y_{d\eta_w} Y^*_{d\eta_w} \Phi_{\eta_w\eta_w}\right\}$$

where $Y_{d\eta_u}(iw)$ is the transfer function from the η_u white noise input to glidepath error, $Y^*_{d\eta_u}$ its complex conjugate, and $\Phi_{\eta_u\eta_u}$ the (constant) power spectral density of the white noise input to the shaping filter.

The optimal control analysis used the tenth-order system model summarized in table A4, with the performance index and weightings that were detailed in the main text. A full-state, optimal-feedback gain matrix was determined using a computer algorithm based on reference 14. The elements of this feedback gain matrix, C, were then modified as shown in table 4 to result in a more practical form for implementation. When the turbulence-shaping filters and the airspeed-complementary filter were incorporated, the feedback control terms formerly involving u and $\int u$ in the optimal solution were similarly reassigned to the filtered quantities, u_f and $\int u_f$. Finally, calculation of the time-response characteristics, the rms statistics, and the power-spectral density functions was carried out as described previously.

REFERENCES

1. Vomaske, R. F., et al.: A Flight Investigation of the Stability, Control, and Handling Qualities of an Augmented Jet Flap STOL Airplane. NASA TP-1254, 1978.

2. Hindson, W. S.; Hardy, G. H.; and Innis, R. C.: A Summary of Joint U.S.-Canadian Augmentor Wing Powered-Lift STOL Research Programs at the Ames Research Center, NASA, 1975-1980. NASA TM-81215, July 1980.

3. Franklin, J. A.; and Innis, R. C.: Flight-Path and Airspeed Control During Approach for a Powered-Lift Aircraft. NASA TN D-7791, 1974.

4. Franklin, J. A.; Innis, R. C.; and Hardy, G. H.: Design Criteria for Flightpath and Airspeed Control for the Approach and Landing of STOL Aircraft. NASA TP-1911, March 1982.

5. Hindson, W. S.; Hardy, G.H.; and Innis, R. C.: Flight-Test Evaluation of STOL Control and Flight Director Concepts in a Powered-Lift Aircraft Flying Curved Decelerating Approaches. NASA TP-1641, March 1981.

6. Hindson, W. S.; Hardy, G. H.; and Innis, R. C.: Flight Experiments Using the Frontside Control Technique During Piloted Approach and Landing in a Powered-Lift STOL Aircraft. NASA TM-81337, 1982.

7. Cleveland, W. B.; Vomaske, R. F.; and Sinclair, S. R. M.: Augmentor Wing Jet STOL Research Aircraft Digital Simulation Model. NASA TM X-62,149, 1972.

8. Feinreich, B.; and Gaevert, G.: Development and Evaluation of Automatic Landing Control Laws for Powered-Lift Aircraft. NASA CR-152399, January 1981.

9. Neuman, F.; and Warner, D. N., Jr.: A STOL Terminal Area Navigation System. NASA TM X-62348, 1974.

10. Feinreich, B., et al.: Development of Automatic Landing Control Laws for Powered-Lift Short Haul Aircraft. AIAA Guidance and Control Conference, Danvers, Mass., August 1980.

11. Chalk, C. R.: Background Information and User Guide for MIL-F-8785B. AFFDL TR-69-72, August 1969.

12. Holley, W. E.; and Bryson, A. E.: Wind Modeling and Lateral Control for Automatic Landing. J. Spacecraft & Rockets, vol. 14, no. 2, February 1977.

13. Bryson, A. E.; and Ho, Y. C.: Applied Optimal Control. Blaisdell Publishing Co., Waltham, Mass., 1969.

14. Mukhopadhyay, V.; Newsom, J. R.; and Abel, I.: A Method for Obtaining Reduced-Order Control Laws for High-Order Systems Using Optimization Techniques. NASA TP-1876, Aug. 1981.

15. Dunn, H. J.: Realizable Optimal Control for a Remotely Piloted Research Vehicle. NASA TP-1654, May 1980.

16. Bryson, A. E.; and Hall, W. E.: Optimal Control and Filter Synthesis by Eigenvector Decomposition. Stanford University, SUDAAR no. 436, November 1971.

17. Etkin, B.: Dynamics of Atmospheric Flight. John Wiley & Sons, New York, 1972.

TABLE 1.- AIRCRAFT STABILITY DERIVATIVES AND CONTROL LAW GAINS

FLIGHT CONDITION: FLAP 65, WEIGHT 191.2 kN (43,000 lb)

δ_{ch_o} = 30 percent δ_{ν_o} = 75 deg δ_{NH_o} = 95.2 percent

HEIGHT 427 m (1400 ft)

ANGLE OF ATTACK 4.5 deg

U_o = 37.1 m/sec (72 kt)

γ_o = −7.5 deg

STABILITY DERIVATIVES

Xu	sec^{-1}	−0.071	Z_u	sec^{-1}	−0.262	M_u	$rps^2/m/sec$	0.0047
X_W	sec^{-1}	0.09	Z_W	sec^{-1}	−0.52	M_W	$rps^2/m/sec$	−0.027
X_{δ_ν}	$m/sec^2/rad$	−1.877	Z_{δ_ν}	$m/sec^2/rad$	−0.368	M_{δ_ν}	sec^{-2}	−0.095
X_q	$m/sec^2/rps$	0	Z_q	$m/sec^2/rps$	−1.18	M_q	sec^{-1}	−1.168
$X_{\delta_{NH}}$	$m/sec^2/percent$	0.014	$Z_{\delta_{NH}}$	$m/sec^2/percent$	−0.385	$M_{\dot{W}}$	$rps^2/m/sec^2$	−0.0121
X_{δ_e}	$m/sec^2/rad$	0	Z_{δ_e}	$m/sec^2/rad$	−1.09	M_{δ_e}	sec^{-2}	−1.082
$X_{\delta_{ch}}$	$m/sec^2/percent$	0	$Z_{\delta_{ch}}$	$m/sec^2/percent$	0.023	$M_{\delta_{ch}}$	$rps^2/percent$	0

CONTROL LAW GAINS

FRONTSIDE SYSTEM			BACKSIDE "TWO CONTROLS"			BACKSIDE "FOUR CONTROLS"		
K_5	rad/m	−0.00172	K_2	rad/m	0.00172	K_1	deg/percent	1.39
K_6	rad/m/sec	−0.00345	K_3	rad/m/sec	0.0142	K_2	rad/m	0.00172
K_7	rad/m-sec	−0.000096	K_6	$deg/m/sec^2$	−1.53	K_4	rad/m/sec	0.19
K_θ	rad/rad	5.0	K_7	deg/m/sec	−2.29	K_5	percent/deg	−10.5
K_q	rad/rps	2.1	K_8	deg/m	−1.145	K_7	deg/m/sec	−3.44
			K_9	deg/m-sec	−0.05	K_8	deg/m	−1.72
			τ_6	sec	0.25	K_9	deg/m-sec	−0.074
						τ_5	sec	10.0

TABLE 2.- EIGENVALUES AND RESIDUES FOR RESPONSES TO AN INITIAL-5m-HEIGHT ERROR FROM GLIDEPATH

EIGENVALUES		RESIDUES				
REAL	IMAGINARY	d	θ	u	δ_{ch}	δ_{ν}
-2.37		1.85	0.099	-0.85	-53.7	-0.59
-0.35		-17.2	0.022	5.2	22.4	0.07
-0.068		4.15	-0.0015	-0.152	-0.104	0.009
-0.745	1.4	6.96	-0.12	-1.53	38.8	0.45
-0.745	-1.4	-1.4	0.104	-0.46	-65.1	-0.63
-0.48	0.09	-6.5	-0.02	-1.01	-10.5	0.17
-0.48	-0.09	16.6	0.004	-15.9	-40.5	-0.97
-0.11	0.065	-5.6	0.02	-1.67	3.14	-0.11
-0.11	-0.065	7.7	-0.013	2.0	0.237	0.048

FRONTSIDE CONFIGURATION

REAL	IMAGINARY	d	θ	u		δ_{NH}
-4.64		-0.017	0.00006	-0.0043		-0.87
-0.054		1.43	-0.0010	-0.057		-0.10
-0.944	1.92	0.014	0.0003	0.022		-2.77
-0.944	-1.92	0.39	-0.0006	-0.045		-3.11
-0.38	0.32	-4.58	0.0053	0.625		2.8
-0.38	-0.32	-8.25	0.0115	0.87		1.34
-0.076	0.062	-1.85	-0.0067	-0.60		0.95
-0.076	-0.062	0.87	-0.0062	0.57		-0.067

BACKSIDE "TWO CONTROL" CONFIGURATION

REAL	IMAGINARY	d	θ	u	δ_{ch}	δ_{NH}
-0.92		8.31	0.0034	-1.8	89.22	16.1
-0.63		-9.42	-0.0078	2.8	-23.1	-5.7
-0.30		-5.11	0.0066	-1.14	2.94	2.04
-0.11		0.18	-0.00003	0.002	1.0	-0.09
-0.05		0.98	-0.0008	0.024	0.0095	-0.05
-0.30		0.05	-0.0014	0.024	0.156	0.035
-1.32	1.37	0.016	0.00002	0.074	-160.5	-12.3
-1.32	-1.37	0.23	0.0001	-0.095	-60.04	-3.26

BACKSIDE "FOUR CONTROL" CONFIGURATION

TABLE 3.- COMPARISON OF RMS PERFORMANCE AND CONTROL ACTIVITY NONLINEAR SIMULATION DATA WITH ANALYSIS RESULTS

		FRONTSIDE SYSTEM		BACKSIDE 2 CONTROLS		BACKSIDE 4 CONTROLS		RESULTS OF "OPTIMAL" CONTROL SYNTHESIS
		EXPT	ANAL	EXPT	ANAL	EXPT	ANAL	ANAL
U_f	knots	1.02	1.31	2.1	1.2	0.95	0.77	0.55
d	m	1.40	1.12	2.01	1.69	1.34	1.22	0.91
$\dot{d}$	m/sec	0.43	0.36	0.42	0.48	0.38	0.41	0.42
θ	deg	1.64	1.41	1.4	0.76[a]	0.8	0.31[a]	1.17
$\dot{\theta}$	deg/sec	0.78	0.65	0.5	a	0.48	0.04[a]	0.59
δ_{NH}	percent	—	—	1.83	1.52	1.38	1.30	0.51
δ_{ν}	deg	10.5	8.0	—	—	4.7	4.4	6.0
δ_{ch}	percent	6.3	5.2	—	—	6.9	6.88	6.8

[a] NOT MEANINGFUL, SINCE PITCHING MOMENT EQUATION NOT MODELED

TABLE 4.- OPTIMAL AND MODIFIED FEEDBACK GAINS AND CORRESPONDING SYSTEM EIGENVALUES

	δ_e		δ_{T_c}		$\delta_{ch}^{\cdot}$		δ_ν		CLOSED LOOP EIGENVALUES	
	"OPTIMAL" GAIN	MODIFIED GAIN	"OPTIMAL" GAIN	MODIFIED GAIN	"OPTIMAL" GAIN	MODIFIED GAIN	"OPTIMAL" GAIN	MODIFIED GAIN	"OPTIMAL" [F - GC]	MODIFIED [F -GC']
u	-0.044	NC	-0.26	NC	3.25	NC	0.277	NC	-1.42	-1.53
$\int u$	-0.0167	NC	0.584	NC	-1.69	NC	0.1074	NC	±1.43j	±1.73j
$\dot{-d}$	-0.0268	-0.036	0.803	0.7035	-12.18	NC	-0.0394	NC	-0.842	-0.667
d	0.0104	NC	-0.673	-0.50	9.0	NC	0.0573	NC	±0.784j	±0.735j
$\int d$	0.00248	NC	-0.173	-0.075	2.056	1.056	0.0114	NC	-0.323	-0.424
q	0.555	NC	-6.91	NC	123.4	NC	-0.458	NC	±0.606j	±0.495j
θ	0.876	NC	-12.44	NC	204.8	NC	-0.978	NC	-0.312	-0.36
$\delta_{NH}^{\cdot}$	0.00196	0.0	-0.059	0.0	0.911	0.0	0.00391	0.0	±0.322j	±0.25j
δ_{NH}	0.00671	NC	-0.2045	NC	3.035	NC	0.0118	NC	-0.586	-0.624
δ_{ch}	-0.000688	NC	0.0171	NC	-0.302	NC	-0.00104	NC	-0.134	-0.361

NC = NO CHANGE

TABLE A1.- SYSTEM MATRIX F FOR THE FRONTSIDE CONFIGURATION

	u	$\int u$	w	δ_{ch}	δ_ν	d	$\int d$	θ	q
$\dot{u}$	X_u	0	X_w	0	X_{δ_ν}	0	0	$-g \cos \gamma_o$	X_q
u	1	0	0	0	0	0	0	0	0
$\dot{W}$	Z_u	0	Z_w	$Z_{\delta_{ch}}$	Z_{δ_ν}	0	0	$Z_{\delta_e} K_\theta - g \sin \gamma_o$	$Z_{\delta_e} Kq + U_o + Z_q$
$\dot{\delta}_{ch}$	0	0	0	$-1/\tau_4$	0	0	0	0	$-K_4$
$\dot{\delta}_\nu$	$-(K_1 X_u + K_2 + K_1/\tau_3$	$-K_2/\tau_3$	$-K_1 X_w$	0	$-1/\tau_3 - X_{\delta_\nu} K_1$	0	0	$K_1 g \cos \gamma_o$	$-K_1 X_q - K_3$
$\dot{d}$	0	0	-1	0	0	0	0	U_o	0
d	0	0	0	0	0	1	0	0	0
$\dot{\theta}$	0	0	0	0	0	0	0	0	1
$\dot{q}$	$M_u + M_{\dot{w}} Z_u$	0	$M_w + M_{\dot{w}} Z_w$	$M_{\dot{w}} Z_{\delta_{ch}}$	$M_{\delta_\nu} + M_{\dot{w}} Z_{\delta_\nu}$	0	0	$K_\theta M_{\delta_e} - {}^{(1)} M_{\dot{w}} g \sin \gamma_o$	$M_q + M_{\delta_e} Kq^{(1)} + M_{\dot{w}} (U_o + Z_q)$

[1] $Z_{\delta_e} K_\theta M_{\dot{w}}$ AND $Z_{\delta_e} K_q M_{\dot{w}}$ TERMS INADVERTENTLY OMITTED.

TABLE A2.- SYSTEM MATRIX [F-GC] FOR THE BACKSIDE "TWO CONTROL" CONFIGURATION

	u	$\int u$	$W - U_o\theta = -\dot{d}$	$X_1 = \delta_{NH}$	δ_{NH}	$X_2 = \delta_{T_c} - (K_6/\tau_6 + K_7)\dot{d}$	d	$\int d$
$\dot{u}$	$X_u + K_3(X_w U_o - g\cos\gamma_o)$	$K_2(X_w U_o - g\cos\gamma_o)$	X_w		$X_{\delta_{NH}}$			
u	1							
$\dot{W} - U_o\dot{\theta}$	$Z_u + K_3(Z_w U_o - g\sin\gamma_o)$	$K_2(Z_w U_o - g\sin\gamma_o)$	Z_w		$Z_{\delta_{NH}}$			
$\dot{X}_1$			$-2.88*(K_6/\tau_6 + K_7)$	-2.8	-4	2.88		
$\dot{\delta}_{NH}$				1				
$\dot{X}_2$			$-(K_8\tau_6 - K_6/\tau_6)/\tau_6$			$-1/\tau_6$	$(K_8 + K_9\tau_6)/\tau_6$	K_9/τ_6
$\dot{d}$			-1					
d							1	

TABLE A3.- SYSTEM MATRIX [F-GC] FOR THE BACKSIDE "FOUR CONTROL" CONFIGURATION

	u	W	d	δ_{NH}	$X_1 = \dot{\delta}_{NH}$	θ	$\int d$	$X_2 = \delta_{ch} - K_5\delta_{T_c} + K_1K_5\delta_{NH}$
$\dot{u}$	$X_u + X_{\delta_\nu}K_4$	X_w		$X_{\delta_{NH}}$		$-g\cos\gamma_o$		
$\dot{W}$	$Z_u + U_oK_2 + Z_{\delta_\nu}K_4$	$Z_w - K_7Z_{\delta_{ch}}K_5$	$K_5K_8Z_{\delta_{ch}}$	$Z_{\delta_{NH}} - K_1K_5Z_{\delta_{ch}}$		$-g\sin\gamma_o + K_5K_7U_oZ_{\delta_{ch}}$	$Z_{\delta_{ch}}K_5K_9$	$Z_{\delta_{ch}}$
$\dot{d}$		-1				U_o		
$\dot{\delta}_{NH}$					1			
$\dot{X}_1$		$-2.88K_7$	$2.88K_8$	-4	-2.8	$2.88K_7U_o$	$2.88\,K_9$	
$\dot{\theta}$	K_2							
$\dot{\int d}$			1					
$\dot{X}_3$		K_5K_7/τ_5	$-K_5K_8/\tau_5$	K_1K_5/τ_5		$-K_5K_7U_o/\tau_5$	$-K_5K_9/\tau_5$	$-1/\tau_5$

TABLE A4.- SYSTEM MATRIX F AND CONTROL TRANSMISSION MATRIX G FOR THE "OPTIMAL" CONTROL SYNTHESIS EXAMPLE

	F MATRIX										G MATRIX			
STATE / CONTROL	U	$\int U$	$W - U_o\theta = -\dot{d}$	d	$\int d$	q	θ	$\delta_{NH}^{\cdot}$	δ_{NH}	δ_{ch}	δ_e	δ_{T_c}	δ_{ch}	δ_{ν}
$\dot{u}$	X_u	0	X_W	0	0	X_q	$X_W U_o - g\cos\gamma_o$	0	$X_{\delta_{NH}}$	0	0	0	0	X_{δ_ν}
$\int\dot{u}$	1	0	0	0	0	0	0	0	0	0	0	0	0	0
$\dot{W} - U_o\dot{\theta}$	Z_u	0	Z_W	0	0	Z_q	$Z_W U_o - g\sin\gamma_o$	0	$Z_{\delta_{NH}}$	$Z_{\delta_{ch}}$	Z_{δ_e}	0	0	Z_{δ_ν}
$\dot{d}$	0	0	-1	0	0	0	0	0	0	0	0	0	0	0
$\int\dot{d}$	0	0	0	1	0	0	0	0	0	0	0	0	0	0
$\dot{q}$	$M_u + M_{\dot{W}}Z_u$	0	$M_W + M_{\dot{W}}Z_W$	0	0	$M_q + M_{\dot{W}}Z_q$	$M_W U_o + M_{\dot{W}}(Z_W U_o - g\sin\gamma_o)$	0	$M_{\delta_{NH}} + M_{\dot{W}}Z_{\delta_{NH}}$	$M_{\dot{W}}Z_{\delta_{ch}}$	$M_{\delta_e} + M_{\dot{W}}Z_{\delta_e}$	0	0	$M_{\delta_\nu} + M_{\dot{W}}Z_{\delta_\nu}$
$\dot{\theta}$	0	0	0	0	0	1	0	0	0	0	0	0	0	0
$\ddot{\delta}_{NH}$	0	0	0	0	0	0	0	-2.8	-4.0	0	0	0	0	0
$\dot{\delta}_{NH}$	0	0	0	0	0	0	0	1	0	0	0	2.88	0	0
$\dot{\delta}_{ch}$	0	0	0	0	0	0	0	0	0	-0.5	0	0	1	0

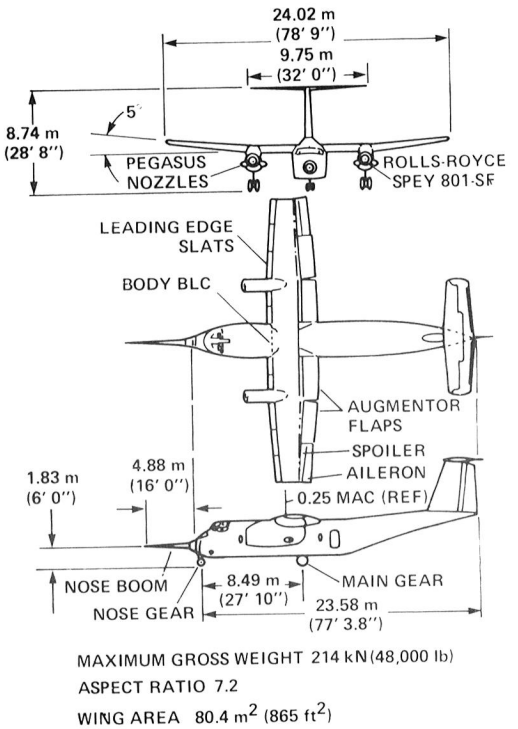

Figure 1.- Augmentor Wing Research Aircraft (AWRA).

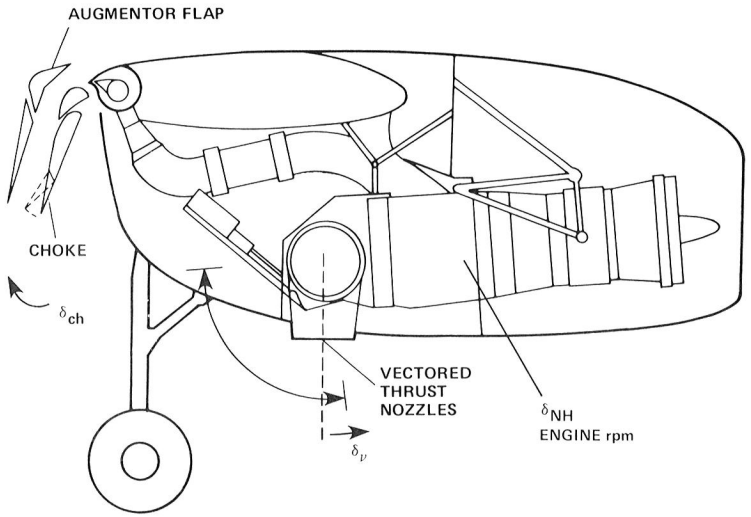

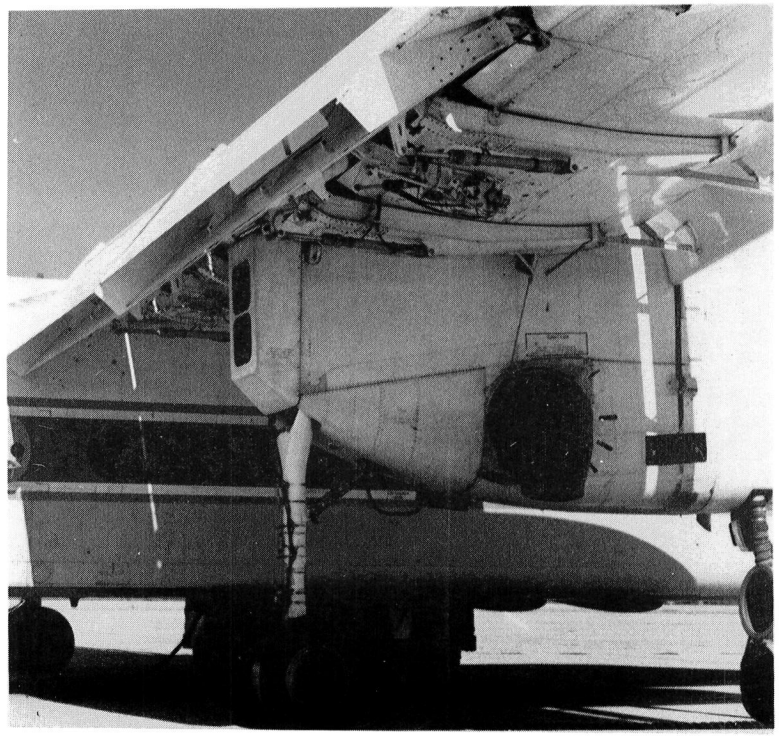

Figure 2.- AWRA powered-lift system and longitudinal controls.

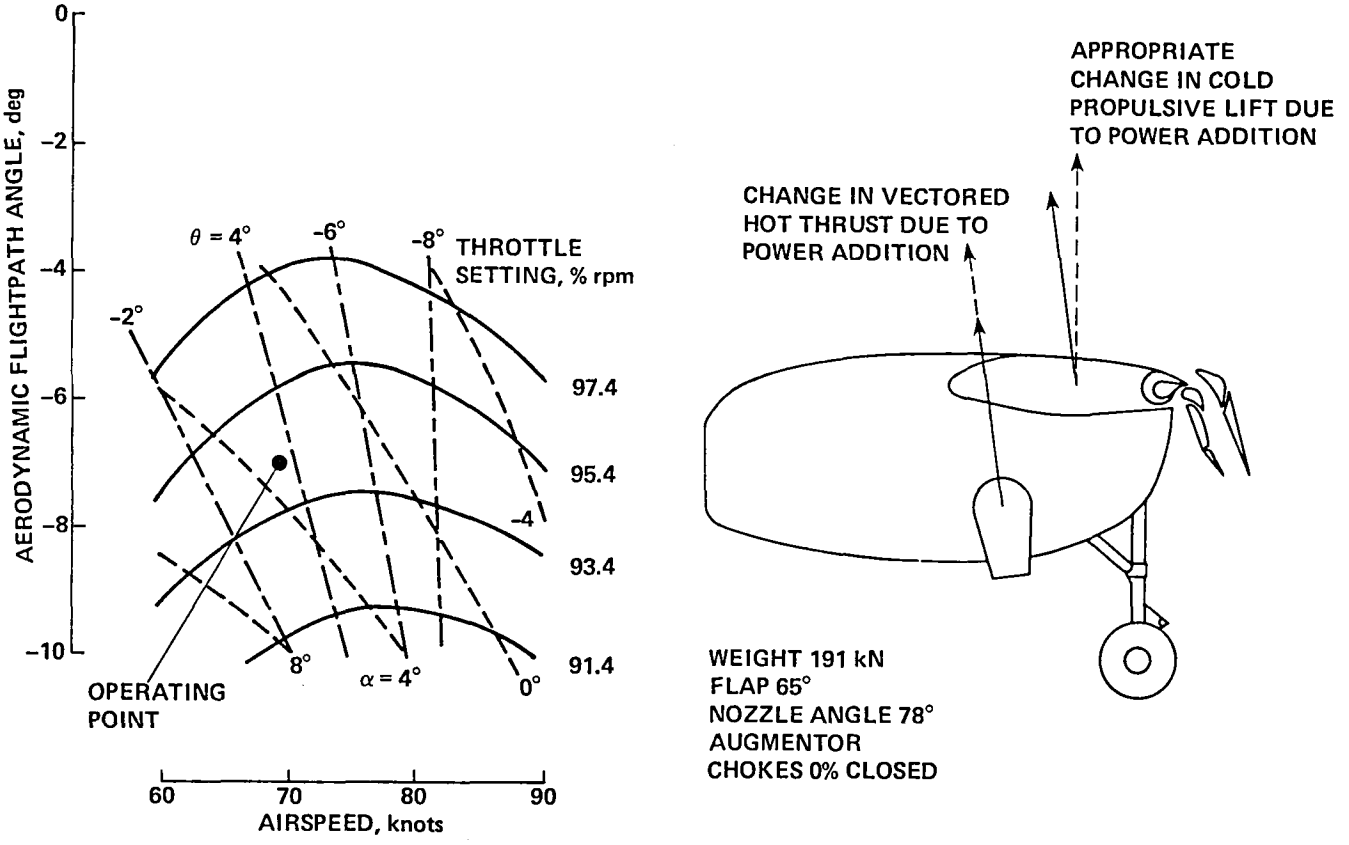

(a) fixed nozzle.

Figure 3.- Approach performance envelope.

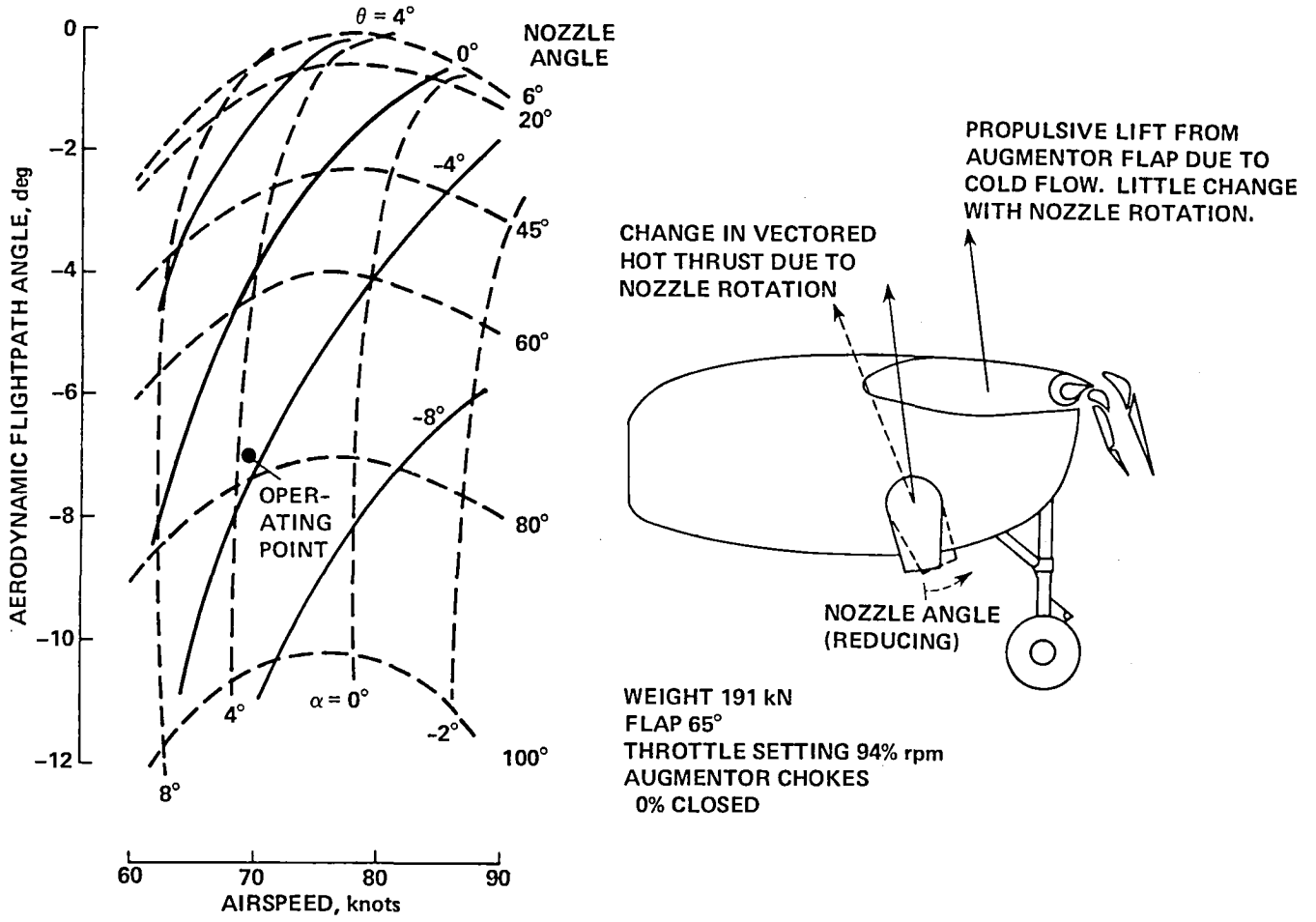

(b) fixed throttle.

Figure 3. - Concluded

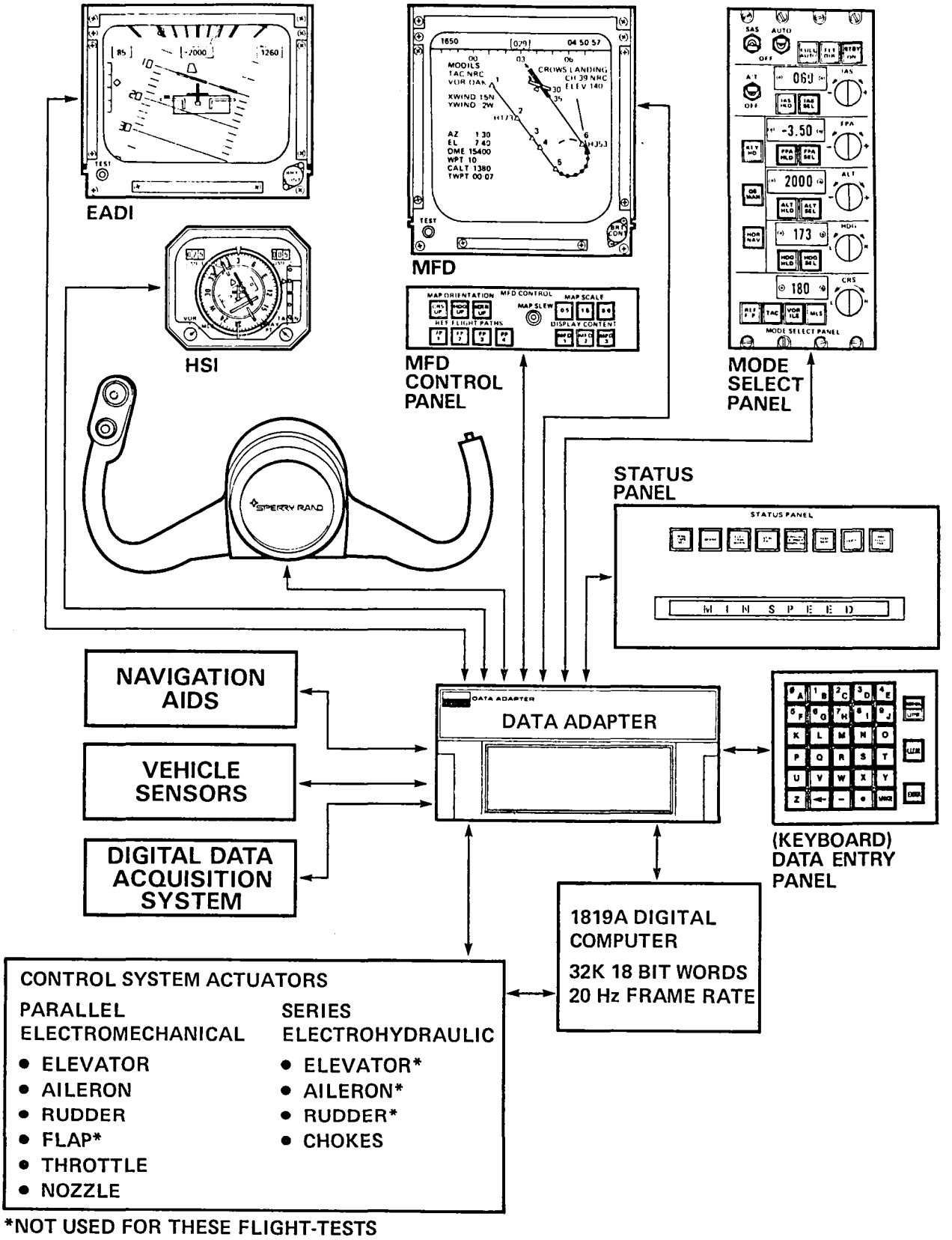

Figure 4.- Research avionics system.

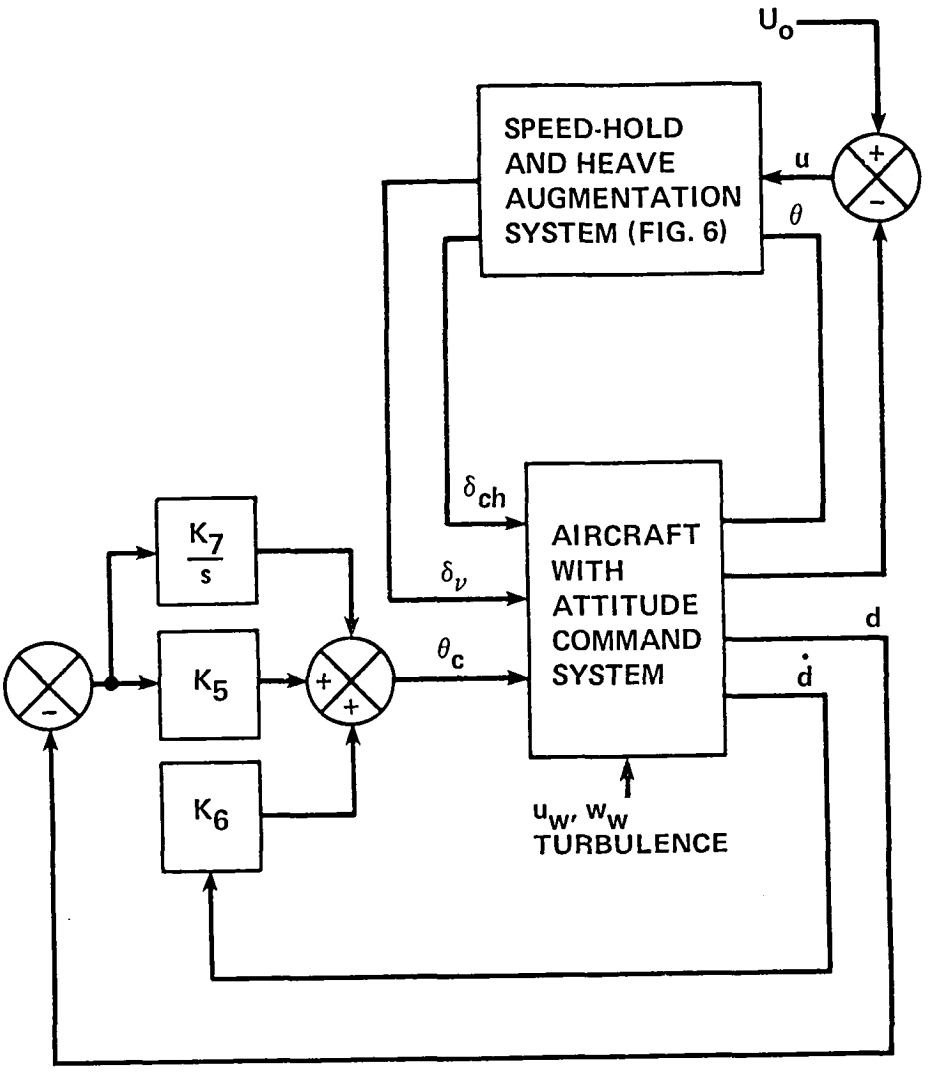

Figure 5.- Glidepath control loop for the frontside configuration.

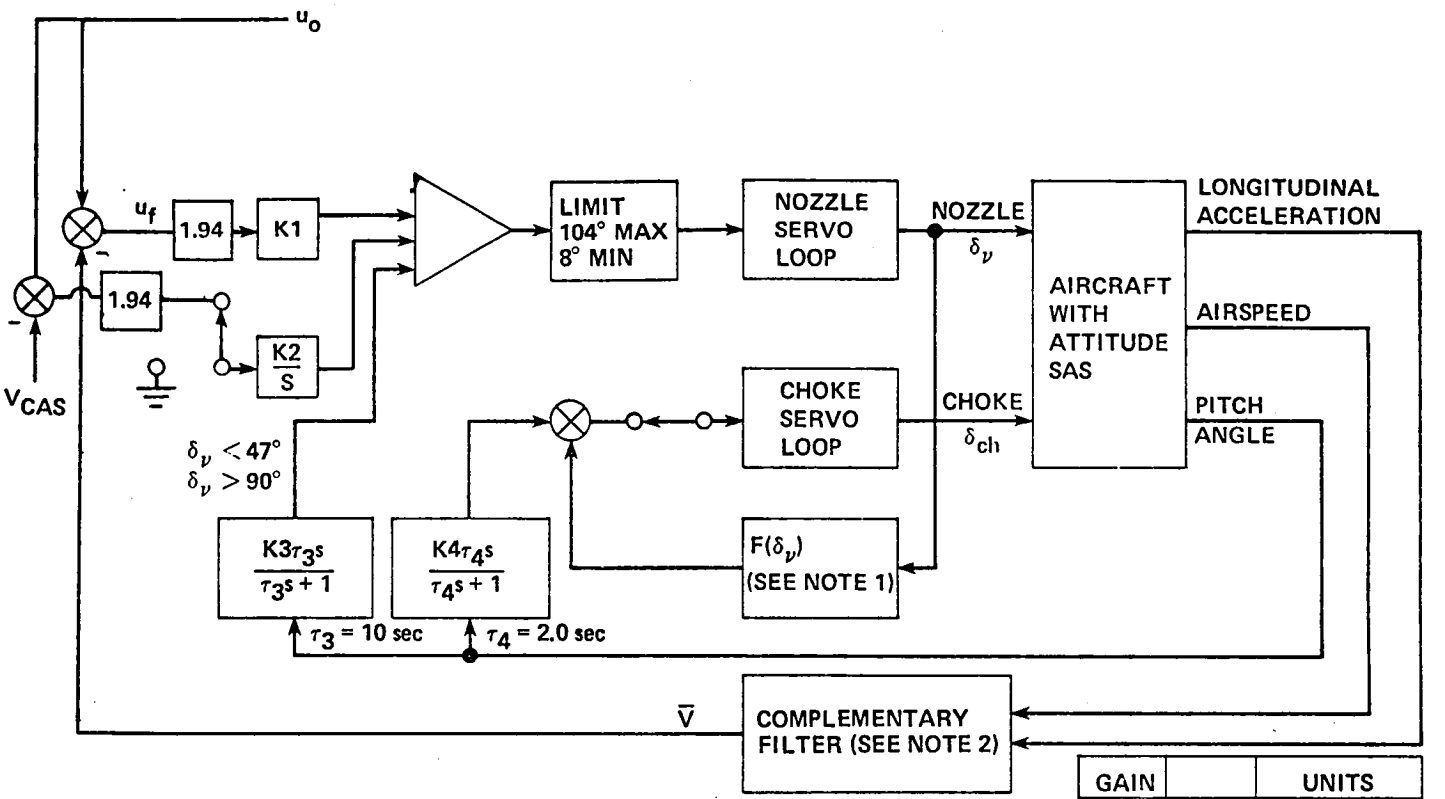

GAIN		UNITS
K1	-9.2	deg/knot
K2	-1.74	deg/knot-sec
K3	-5.0	deg/deg
K4	-7.5	percent/deg
K5	0.75	percent/deg

NOTES: 1. CHOKE SCHEDULING TO COMPENSATE NOZZLE LIFT LOSS

$$F(\delta_v) = \left\{ K5\,(\delta_\nu - \delta_{\nu_{TRIM}}) + 30 \right\} \Big|_{\text{max} = 40\% \text{ closure}}$$

2. AIRSPEED COMPLEMENTARY FILTER

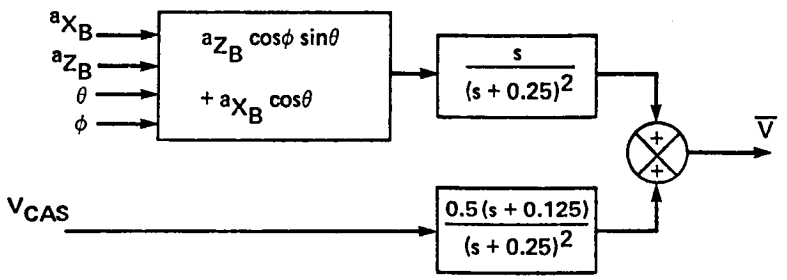

Figure 6.- Speed-hold system used for the frontside configuration.

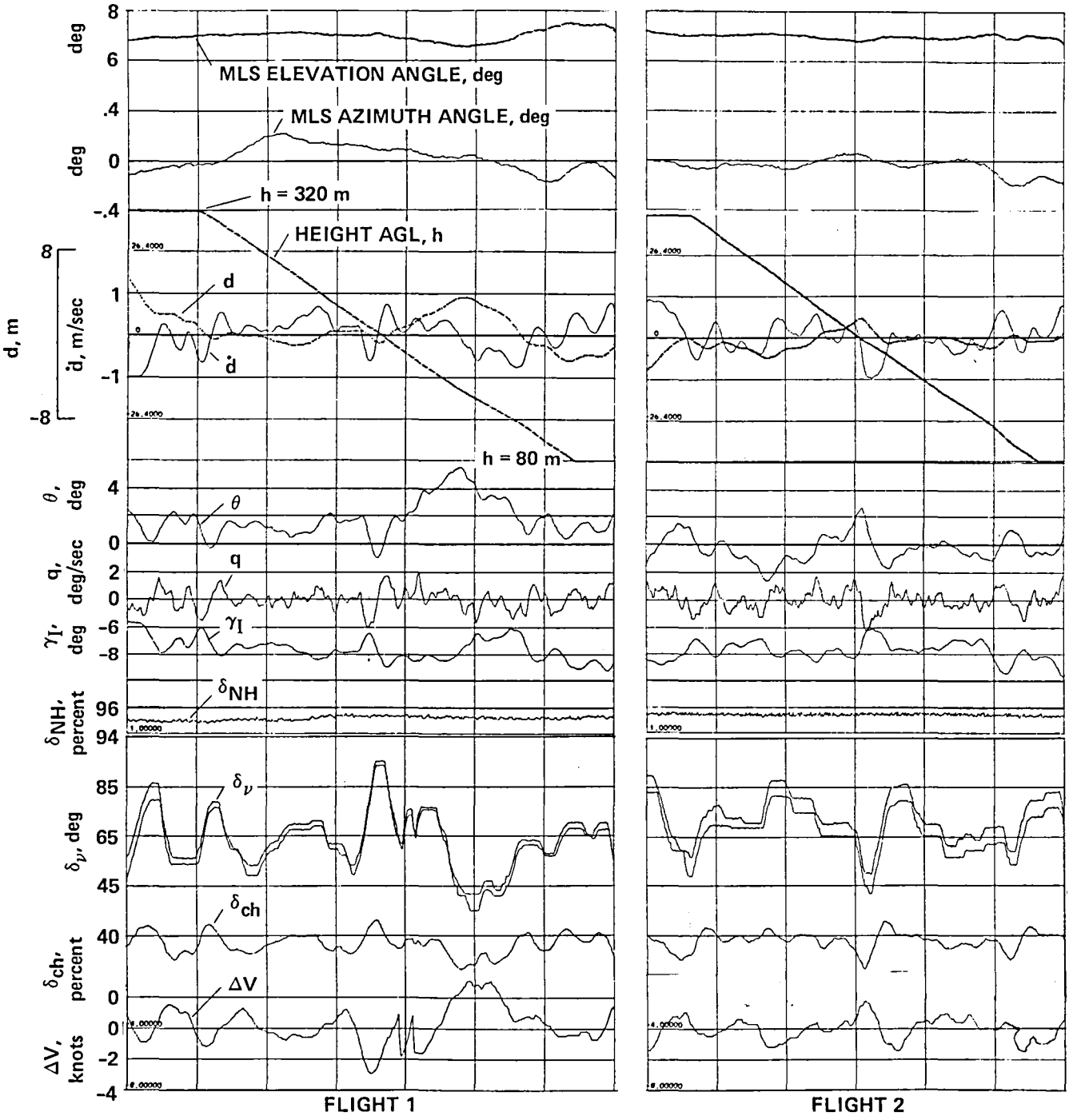

Figure 7.- Approach time histories from flight test-frontside configuration.

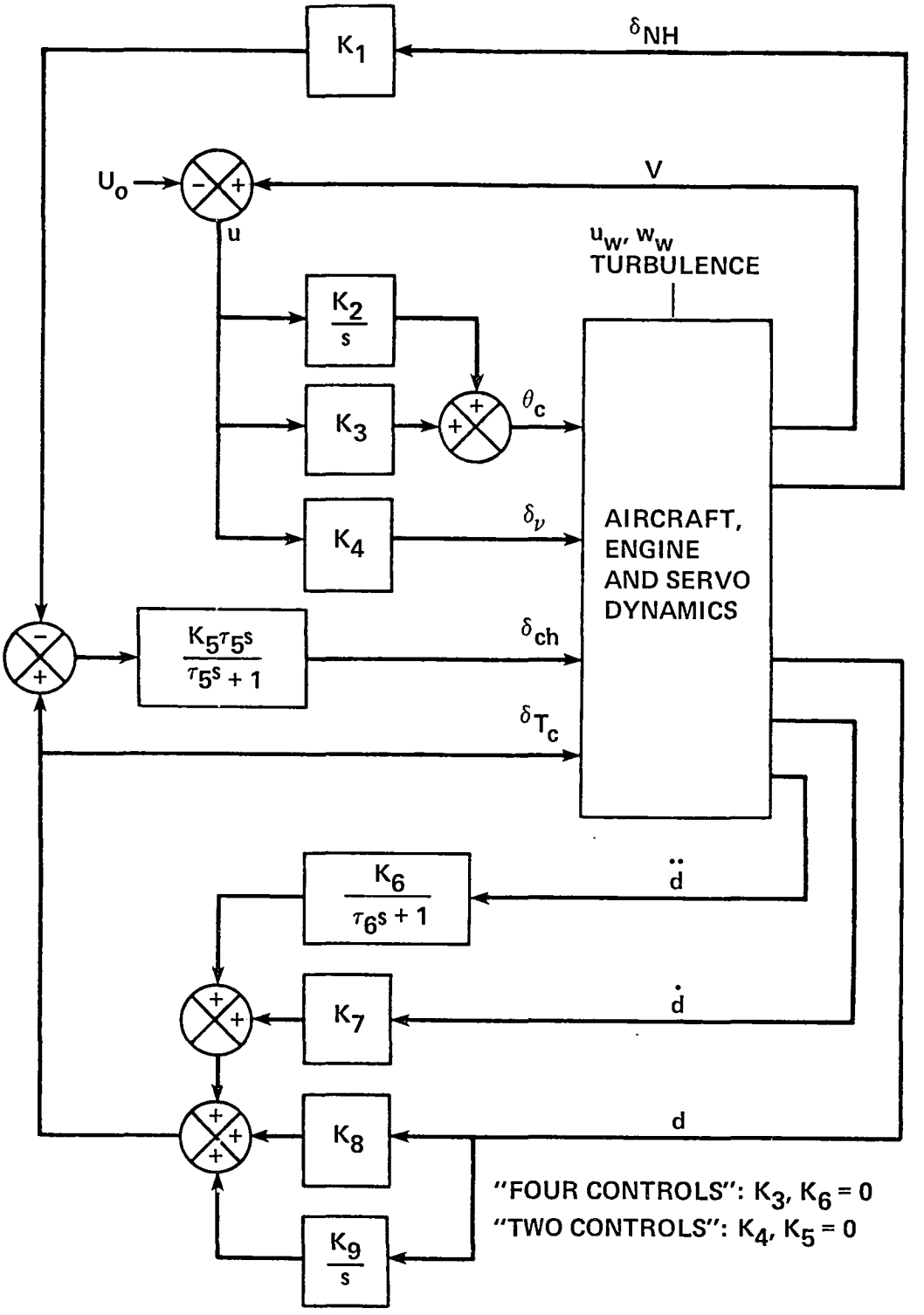

Figure 8.- Glidepath control loop for the backside configurations.

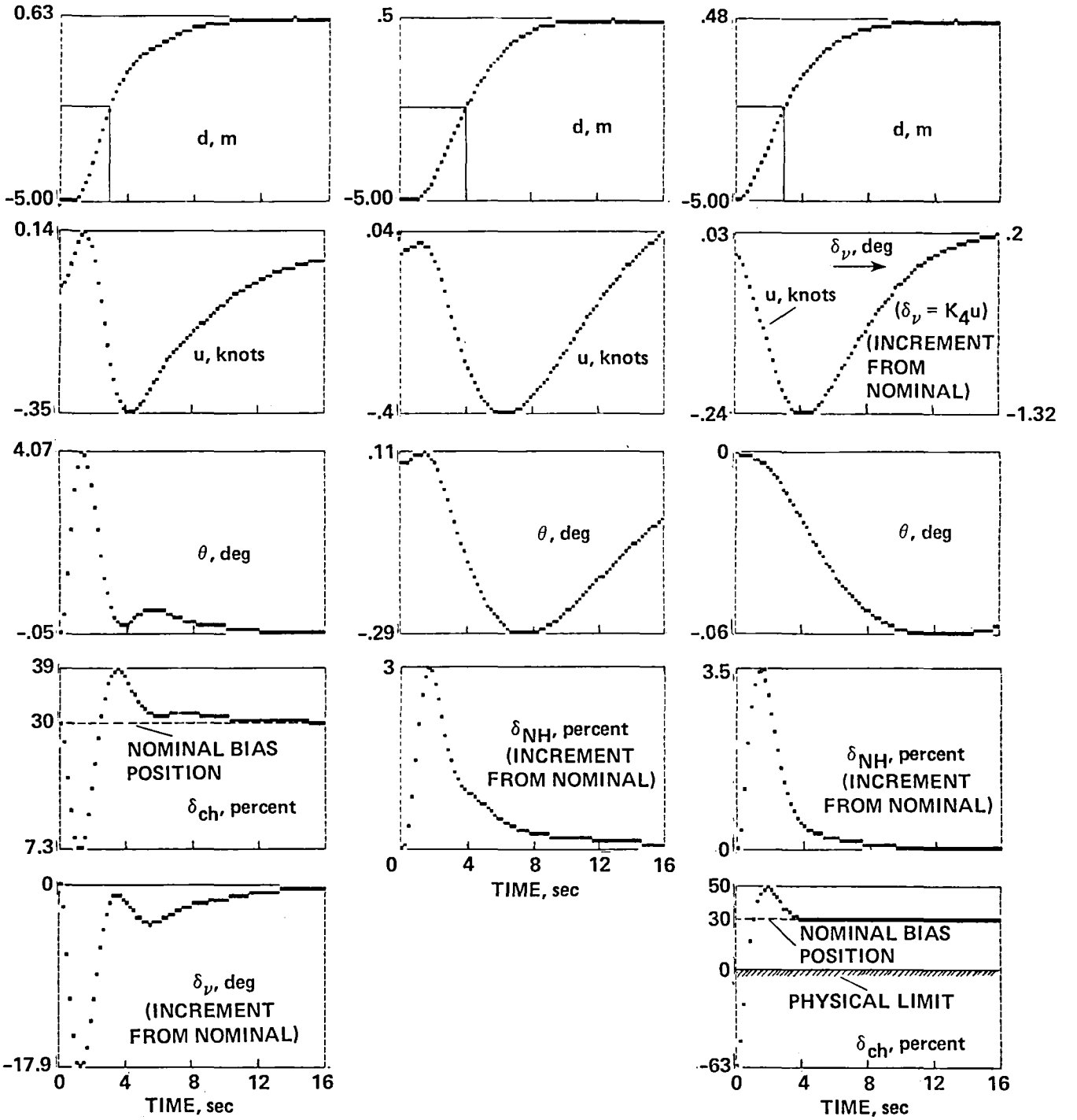

(a) Frontside configuration.

(b) Backside "two control" configuration.

(c) Backside "four control" configuration.

Figure 9. - System response time histories to initial offset 5 m below glidepath.

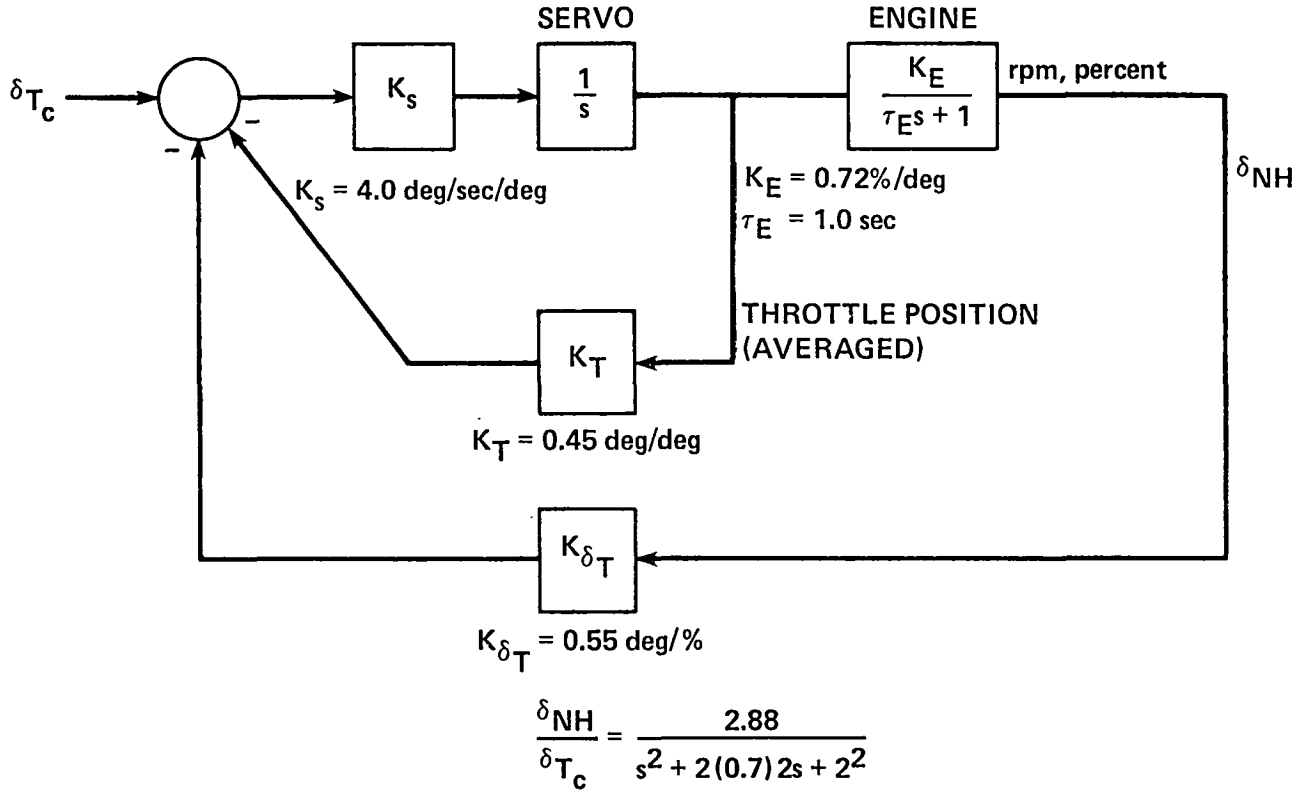

Figure 10.- Throttle servo and engine model used for backside configurations.

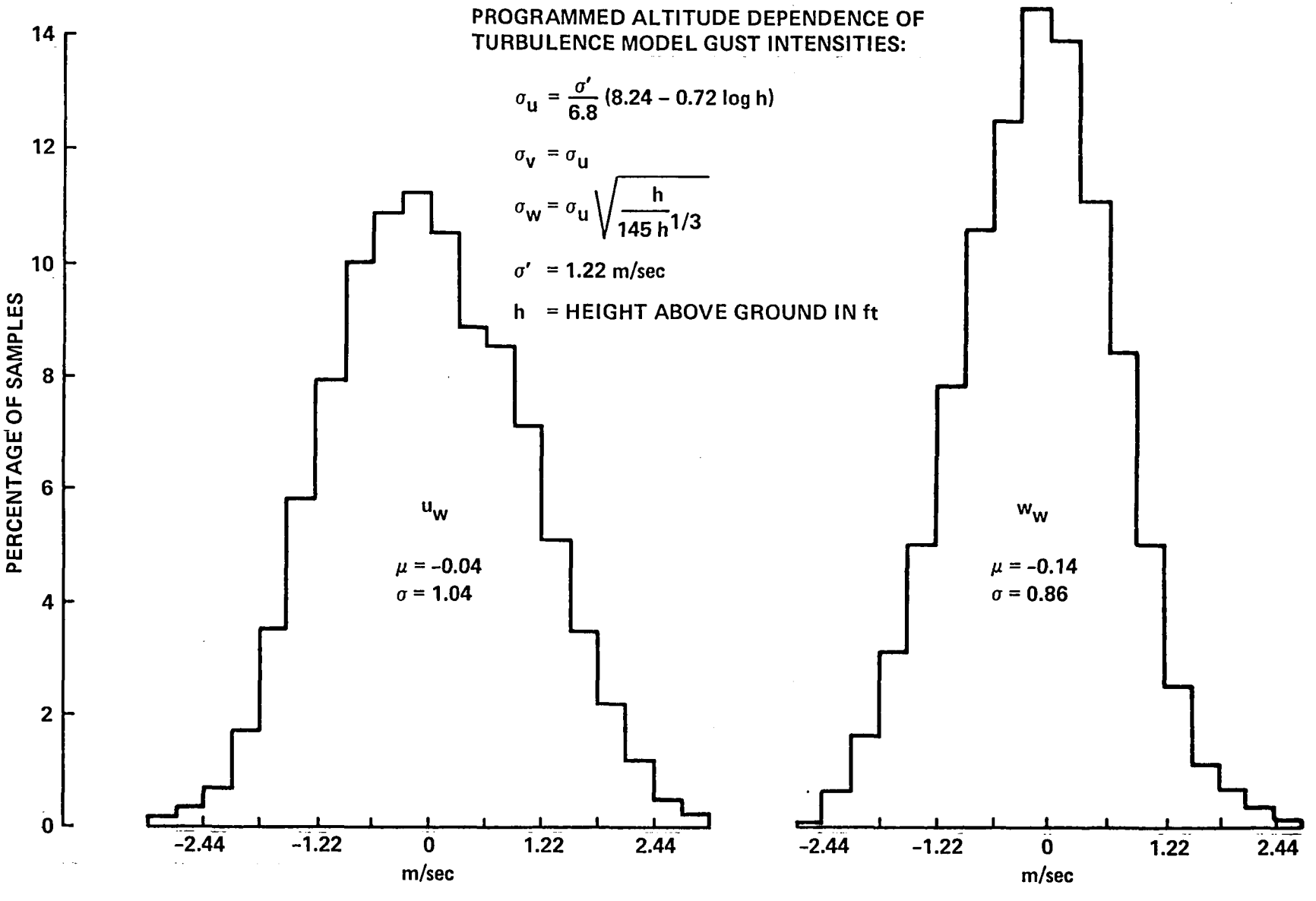

Figure 11.- Accumulated distributions of simulated turbulence model gust intensities during 43 approaches between 500 m and 50 m.

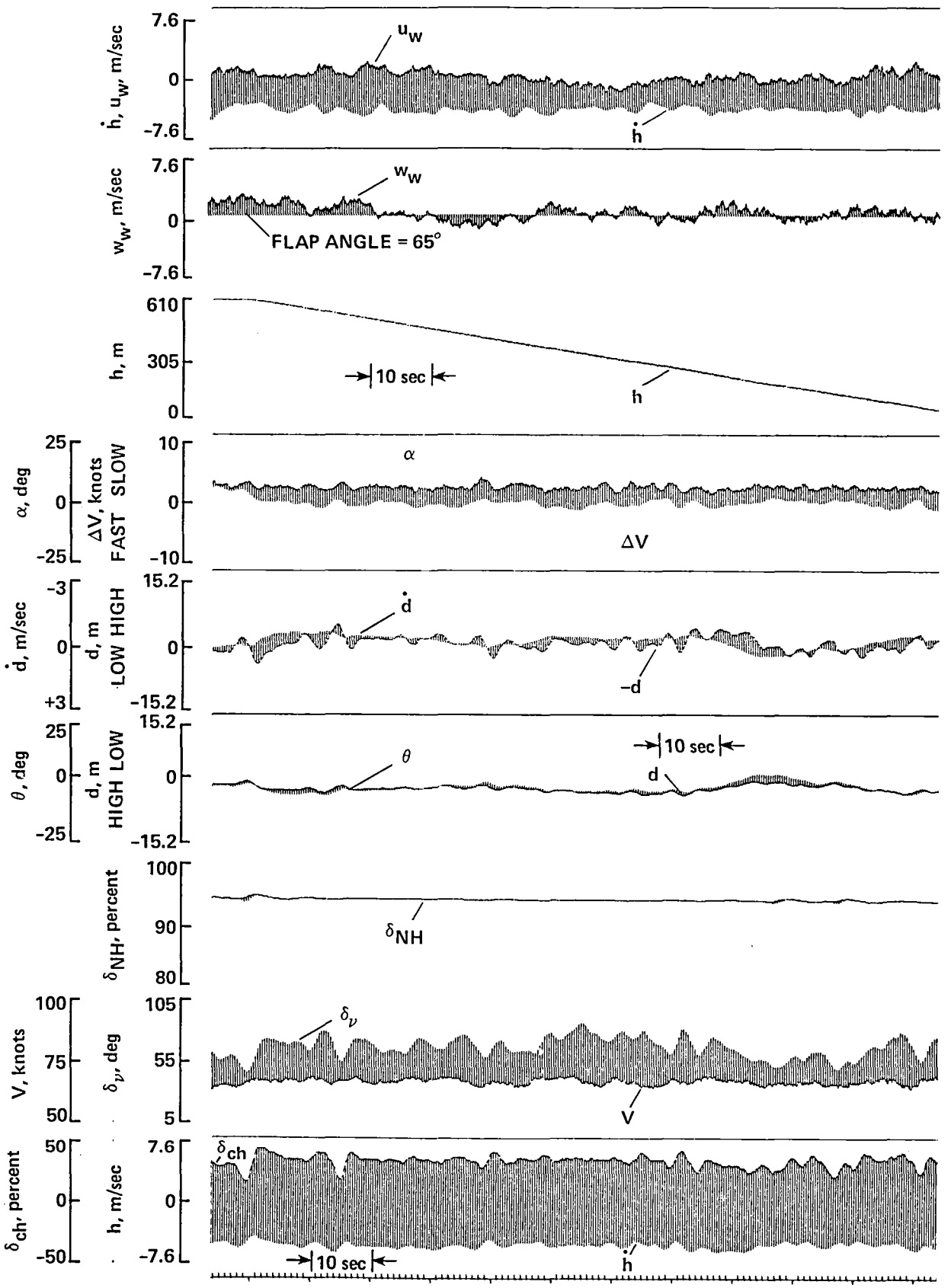

(a) frontside configuration.

Figure 12.- Typical response time histories from simulated approaches in turbulence

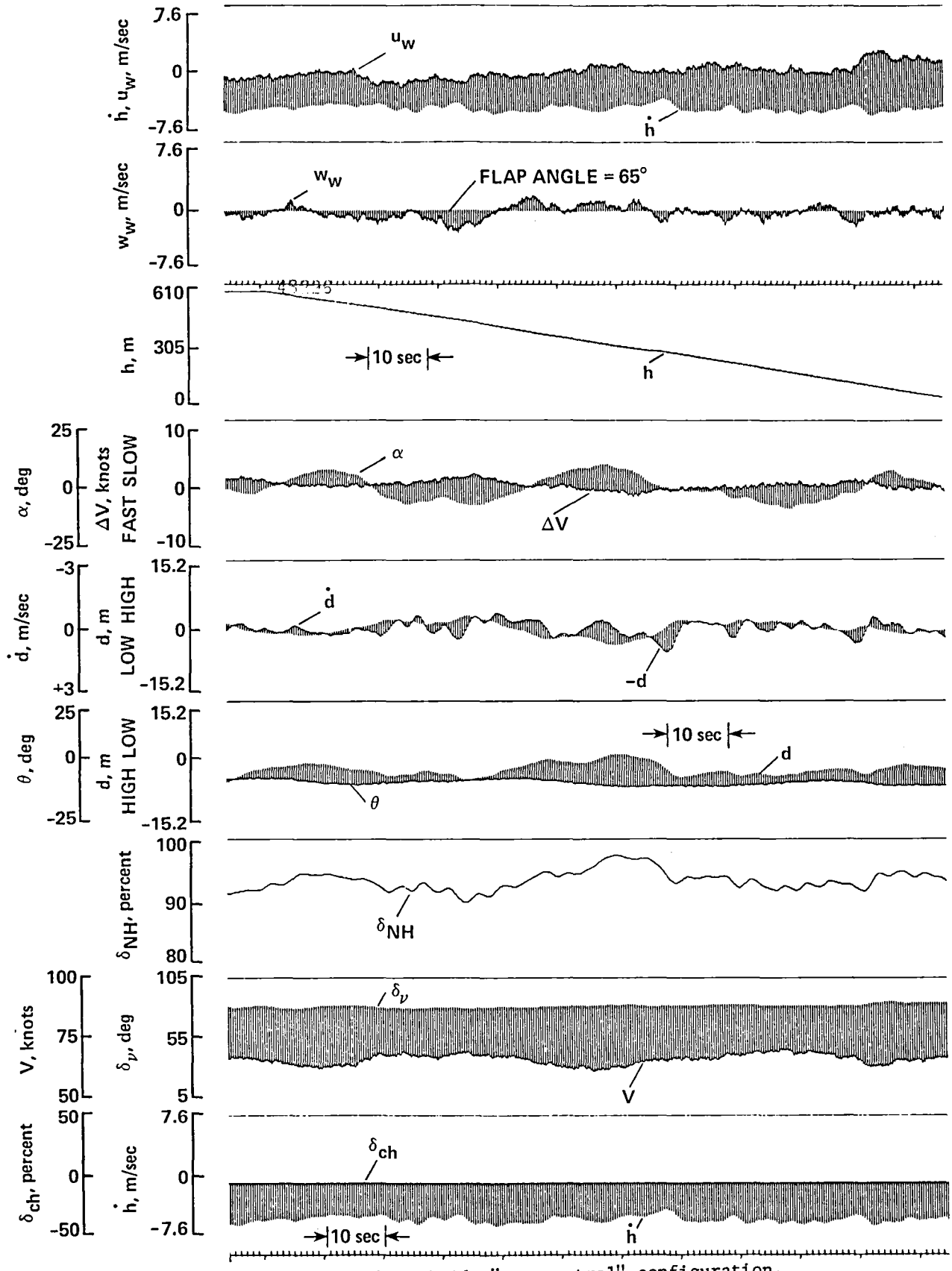

(b) backside "two control" configuration.

Figure 12 Continued.

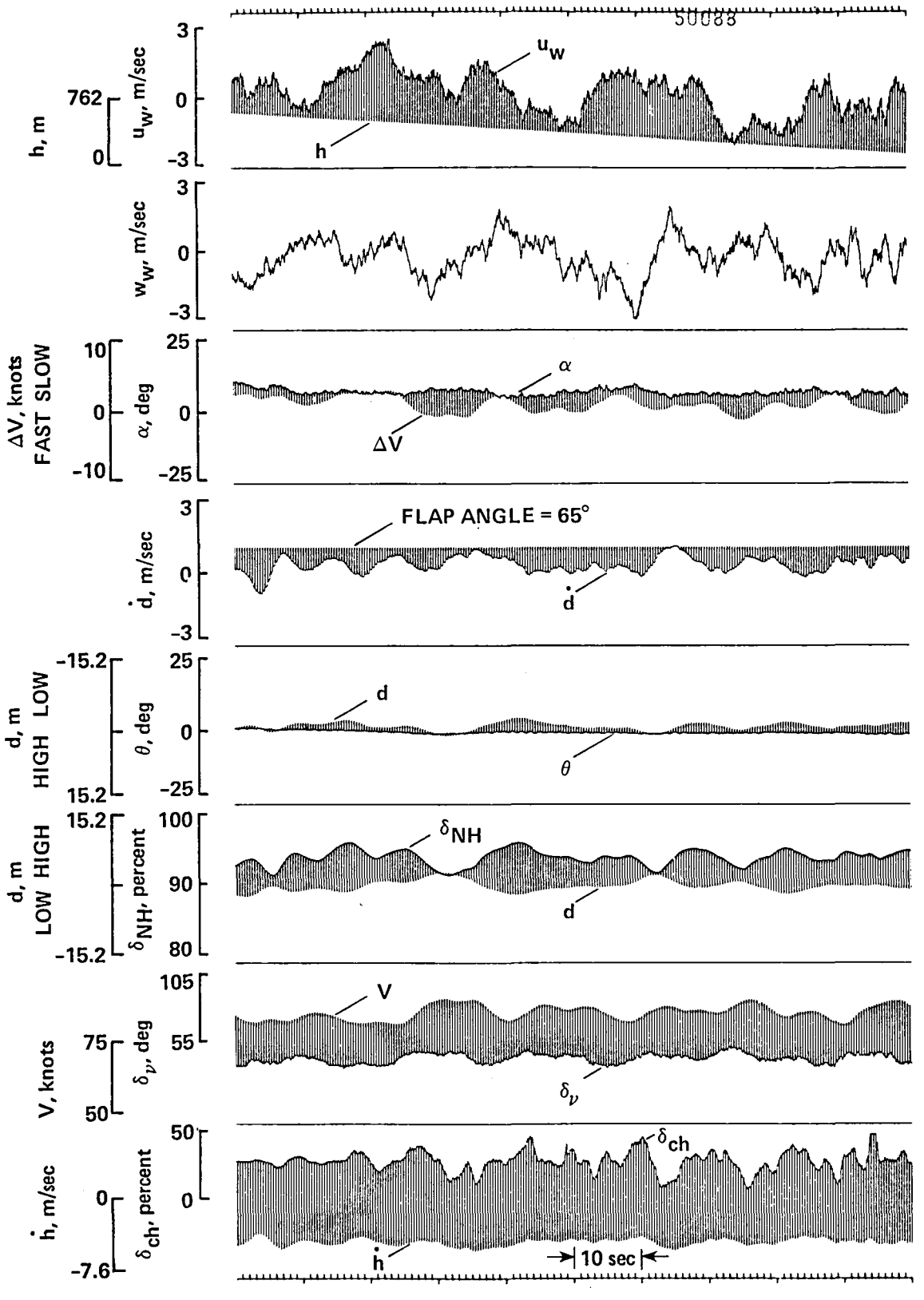

(c) backside "four control" configuration.

Figure 12. - Concluded

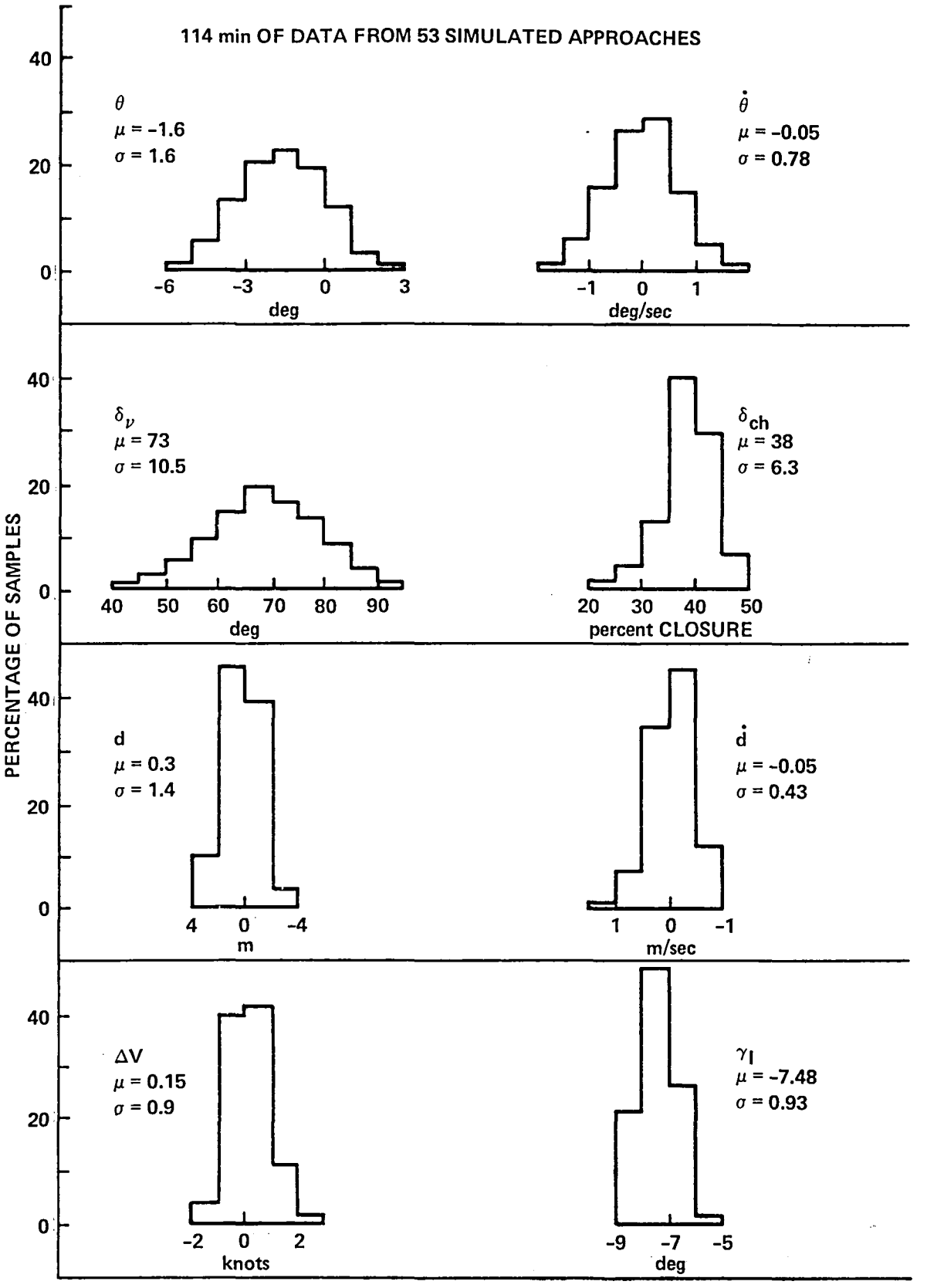

(a) frontside automatic control system

Figure 13.- Histograms of performance and control utilization data in simulated turbulence.

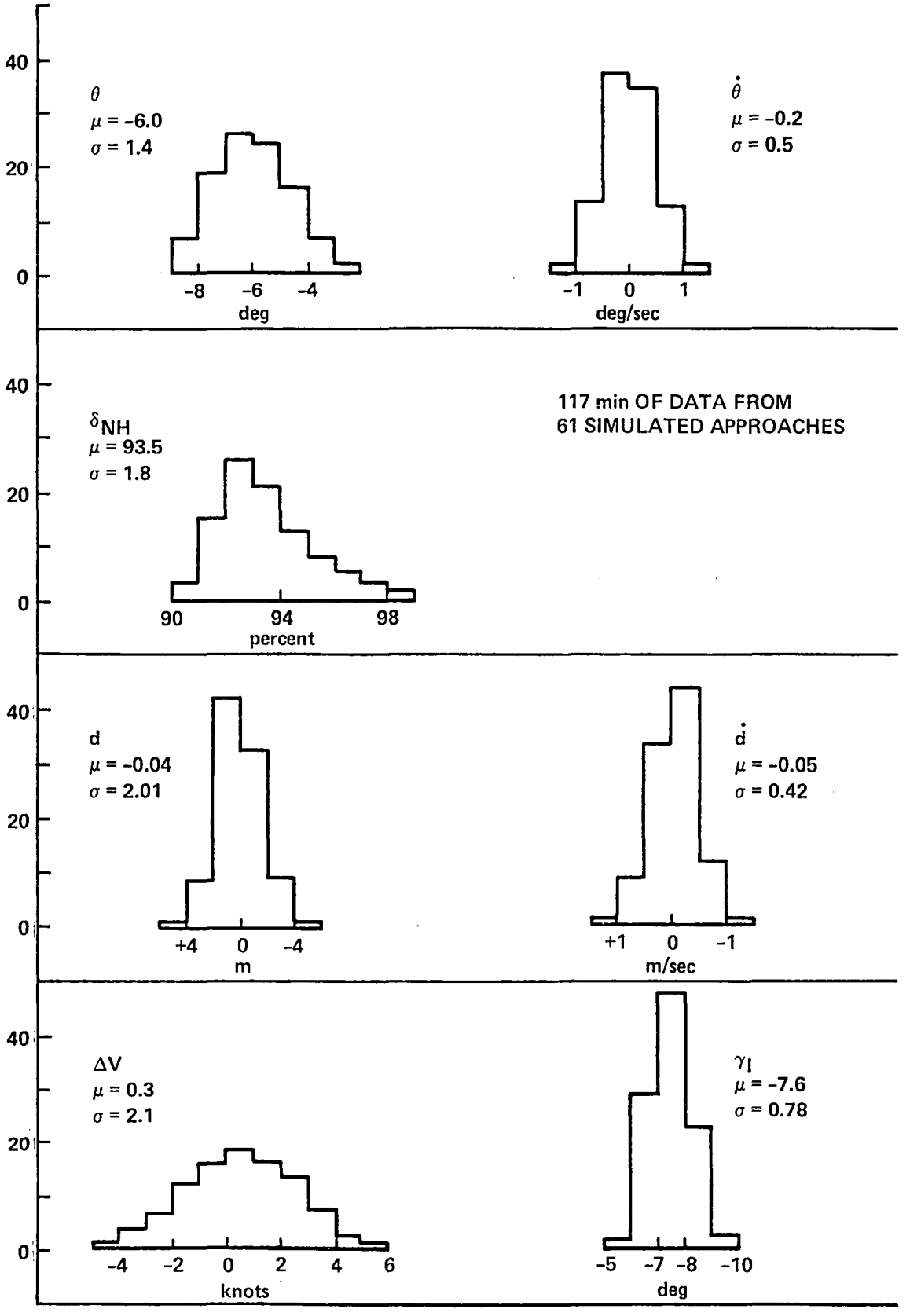

(b) backside automatic control system (two controls).

Figure 13. - Continued

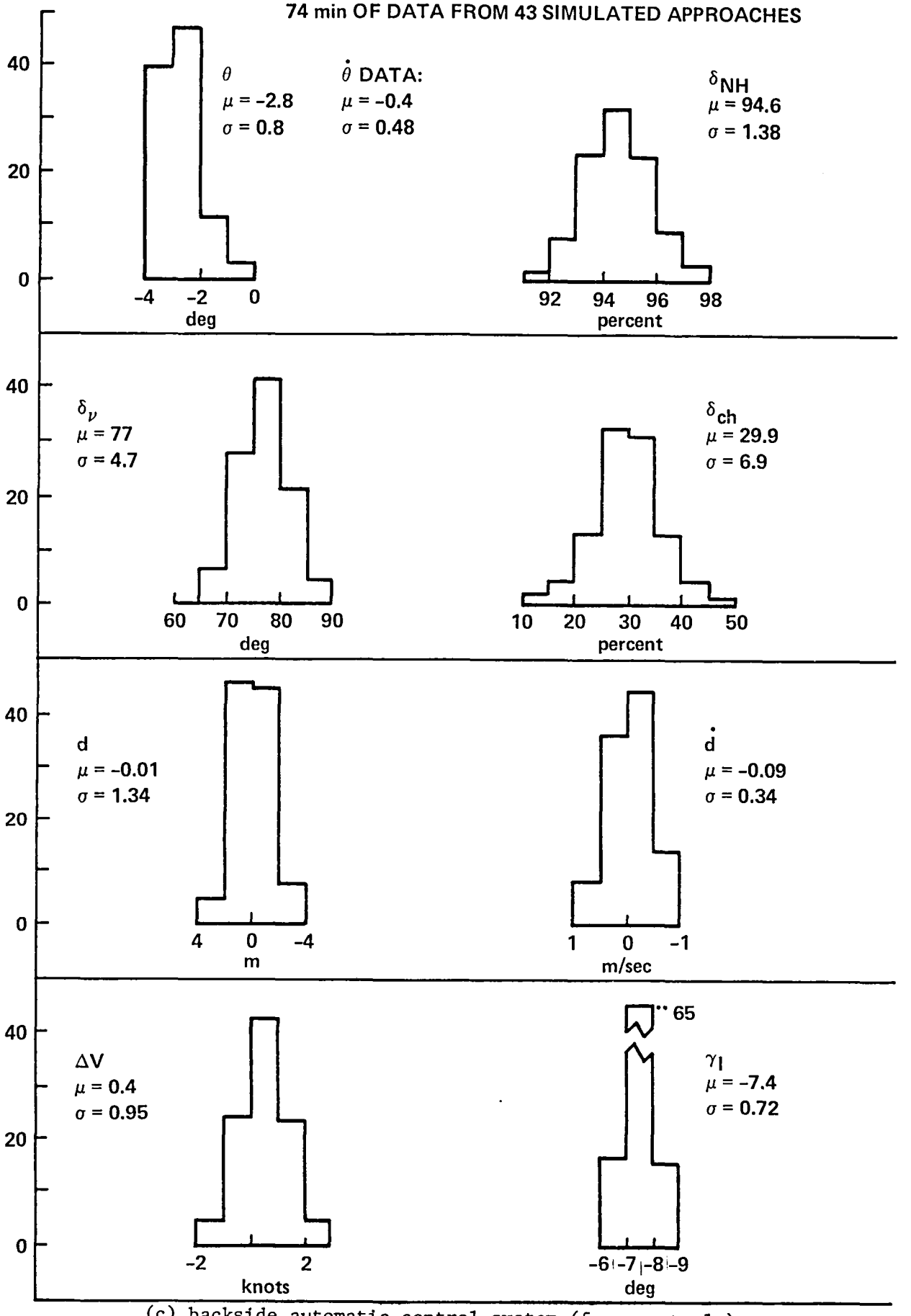

(c) backside automatic control system (four controls).

Figure 13. - Concluded

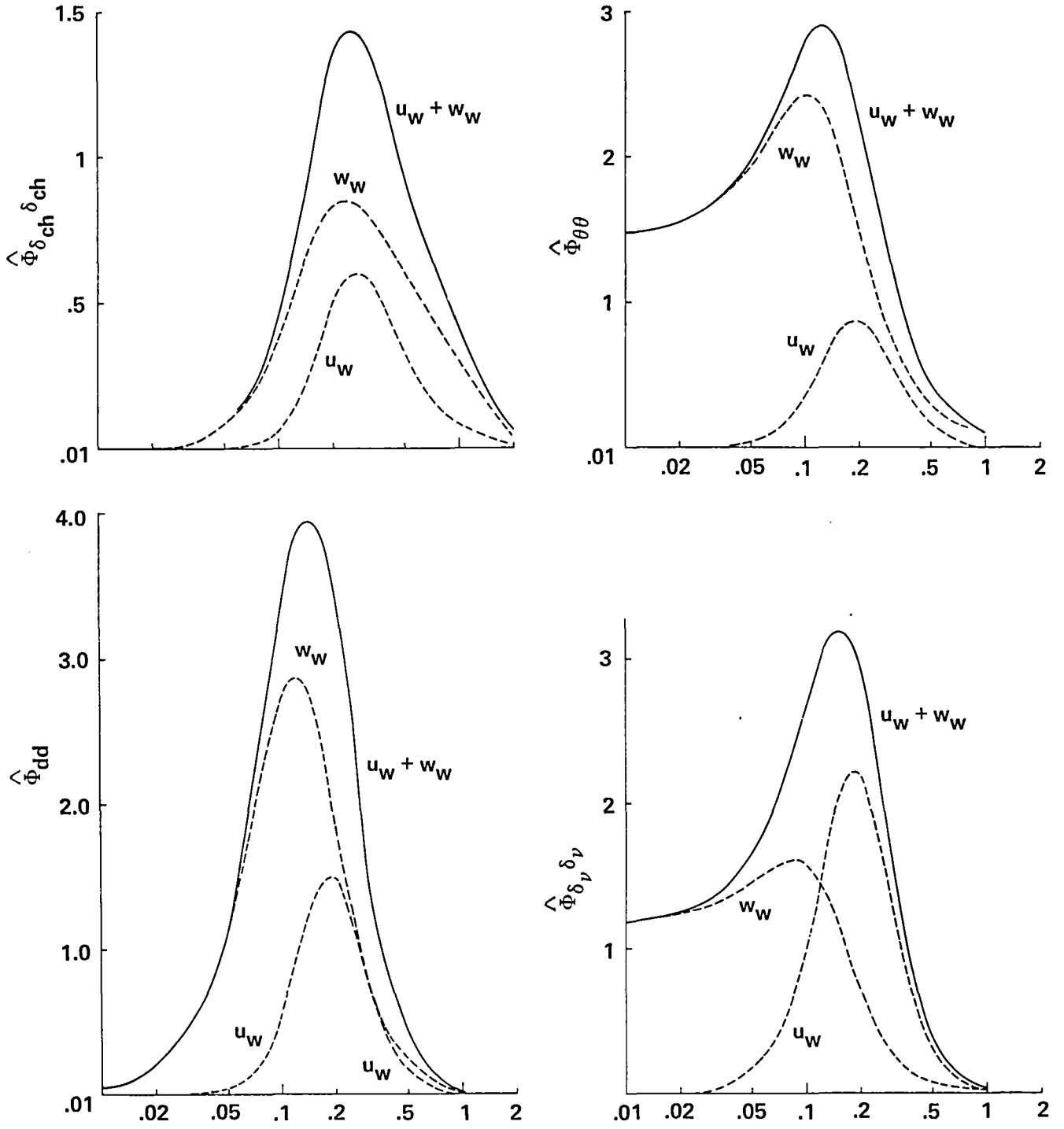

(a) frontside automatic control system

Figure 14.- Power spectral density functions of performance and control utilization in simulated turbulence.

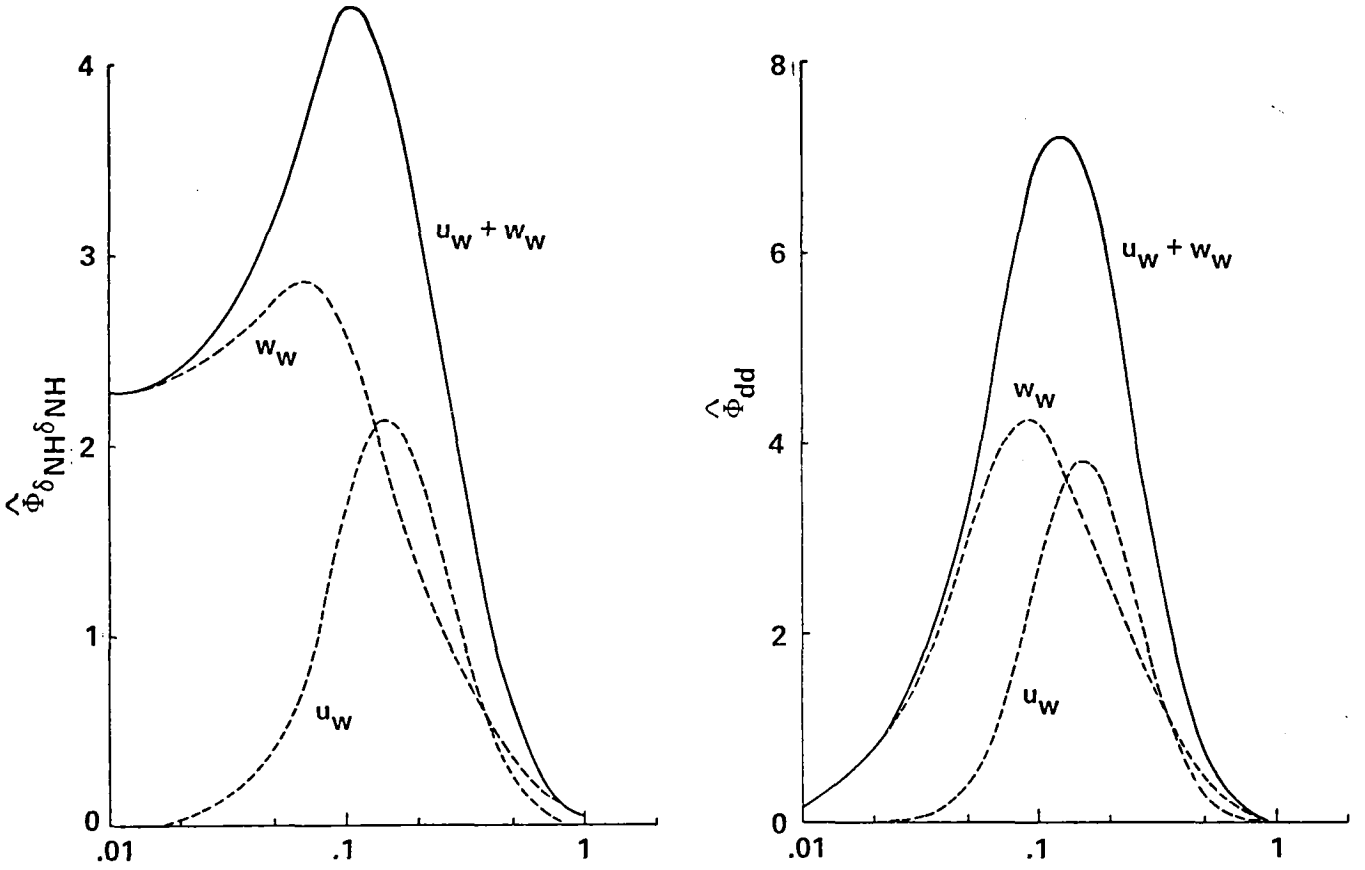

(b) backside automatic control system (two controls).

Figure 14. - Continued

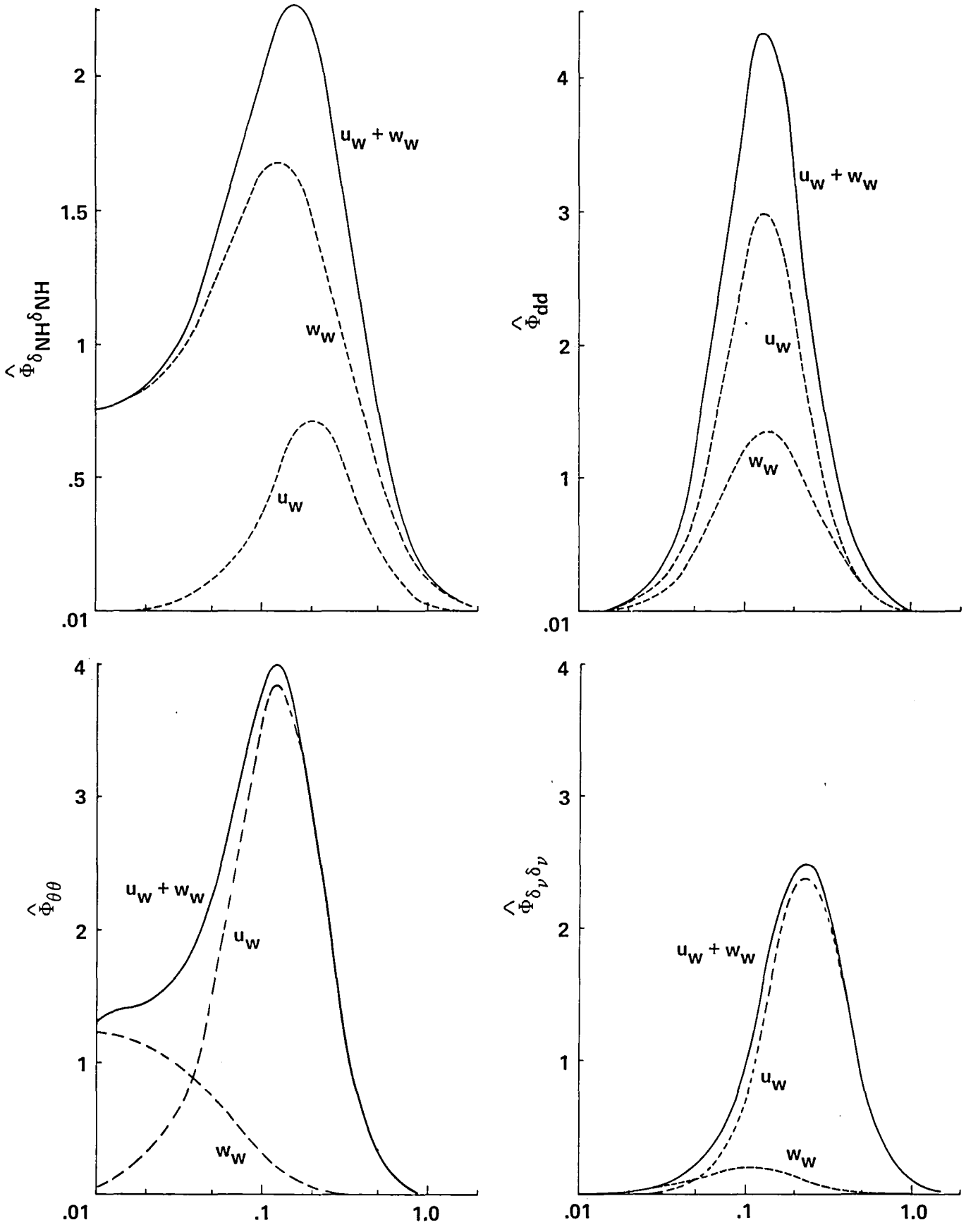

(c) backside automatic control system (four controls).

Figure 14. - Concluded

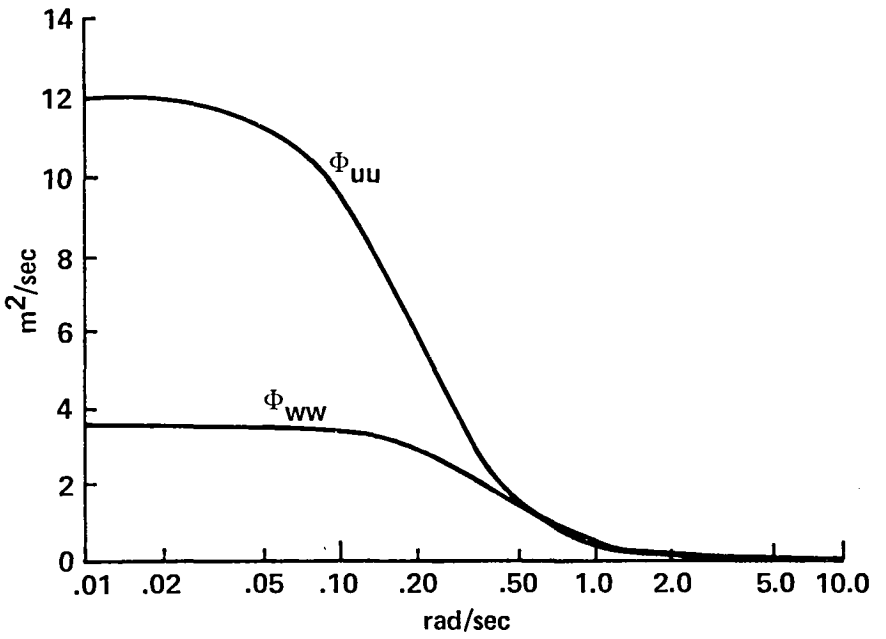

Figure 15.- Power spectral density of simulated turbulence inputs.

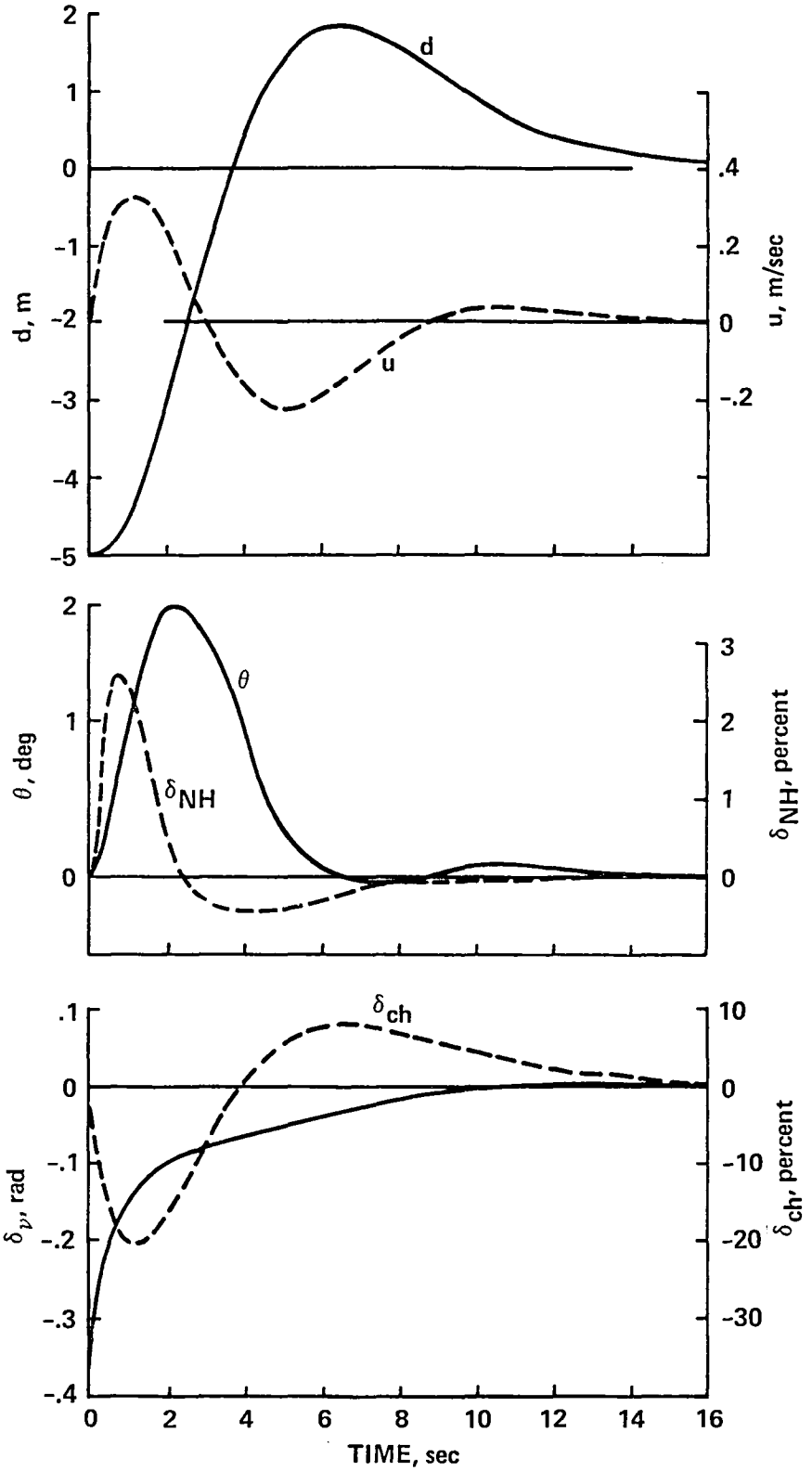

Figure 16.- Transient response to an initial 5 m offset below glidepath — optimal control law.

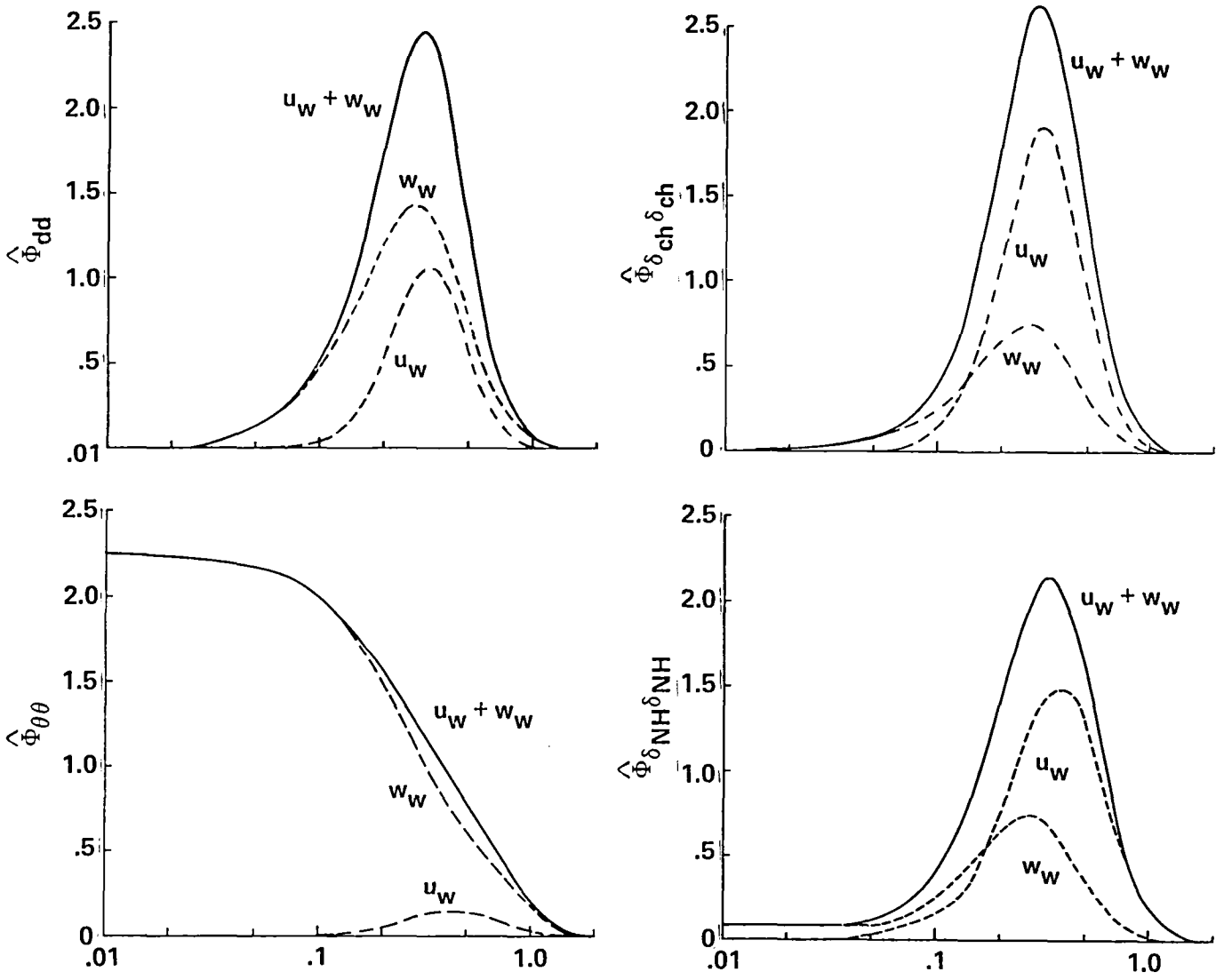

Figure 17.- Power spectral density functions for the optimal control design.

1. Report No.	2. Government Accession No.	3. Recipient's Catalog No.
NASA TM-84282		

4. Title and Subtitle	5. Report Date
ANALYSIS OF SEVERAL GLIDEPATH AND SPEED CONTROL AUTOPILOT CONCEPTS FOR A POWERED-LIFT STOL AIRCRAFT	August 1982
	6. Performing Organization Code

7. Author(s)	8. Performing Organization Report No.
W. S. Hindson	A-9005
	10. Work Unit No.
	T-3847Y
9. Performing Organization Name and Address	11. Contract or Grant No.
NASA Ames Research Center Moffett Field, CA 94035	
	13. Type of Report and Period Covered
12. Sponsoring Agency Name and Address	Technical Memorandum
National Aeronautics and Space Administration Washington, D.C. 20546	14. Sponsoring Agency Code 533-02-01

15. Supplementary Notes

Point of Contact: W. S. Hindson, MS 211-2, Ames Research Center, Moffett Field, CA 94035, (415) 965-5008 or FTS 448-5008

16. Abstract

A comparison of longitudinal performance and control utilization data is provided for several different automatic-approach autopilot implementations in a powered-lift STOL aircraft. As few as two, to as many as four longitudinal controls are used to manage glidepath and speed with control laws reflecting both backside and frontside control techniques. The data are developed from analysis and simulation, but represent configurations which had actually been demonstrated in flight. Transient response characteristics from initial glidepath offsets are presented, along with performance and control statistics, and spectral content descriptive of system operation in turbulence. In furnishing quantitative data in controlled levels of simulated turbulence, these results provide a useful supplement to various flight investigations (including those employing manual control) that have involved a comparison of control techniques in this type of aircraft.

17. Key Words (Suggested by Author(s))	18. Distribution Statement
Automatic Control Control Technique Powered-Lift STOL	Unlimited Subject Category 08

19. Security Classif. (of this report)	20. Security Classif. (of this page)	21. No. of Pages	22. Price*
Unclassified	Unclassified	55	A02

*For sale by the National Technical Information Service, Springfield, Virginia 22161